minerals

MDPI

Article

Geometallurgical Characterization of Non-Ferrous Historical Slag in Western Tasmania: Identifying Reprocessing Options

Anita Parbhakar-Fox [1,2,*], Sarah Gilmour [3], Nathan Fox [1] and Paul Olin [2,4]

1 W.H.Bryan Mining and Geology Research Centre, Sustainable Minerals Institute, University of Queensland, 40 Isles Road, Indooroopilly, Brisbane, QLD 4068, Australia
2 Centre for Ore Deposit and Earth Sciences (CODES), University of Tasmania, Private Bag 79, Sandy Bay, TAS 7001, Australia
3 GHD (Gutteridge, Haskins and Davey), 2 Salamanca Square, Battery Point, TAS 7000, Australia
4 ARC Transforming the Mining Value Chain (TMVC) Industrial Transformation Research Hub, University of Tasmania, Private Bag 79, Sandy Bay, TAS 7001, Australia
* Correspondence: a.parbhakarfox@uq.edu.au; Tel.: +61-07-3365-5977

Received: 1 May 2019; Accepted: 3 July 2019; Published: 5 July 2019

Abstract: Pyrometallurgical processing of ore from the Zeehan mineral field was performed intermittently between 1896 and 1948, primarily recovering Pb, Ag and Cu. While Zn recovery was attempted at the time, it was unsuccessful using the available technology. Consequently, Zn reported to the slag during the smelting process. Today, the former smelter site consists of two large slag piles (North and South). Using a range of techniques (including X-ray diffractometry, scanning electron microscopy, laser ablation inductively coupled plasma mass spectrometry, and static testing) the geometallurgical and geo-environmental properties of these slag materials (n = 280) were determined. The South and North piles contain on average 15% and 11% Zn, respectively. A range of complex mineral phases were identified, and are dominated by glass, silicates (i.e., monticellite–kirschsteinite and hardystonite), oxides (gahnite and hercynite) and minor sulfides (sphalerite and wurtzite). Microtextural examinations defined nine mineral phases (Glass A, Silicates A to D, Oxides A and B, Sulfides A and B). Zn was concentrated in Sulfide A (26%), Glass A (24%) and the Silicates (43%), while Pb was concentrated in Oxide B (76%), with Sulfide B host to the highest Ag (45%) and Cu (65%). Considering this, recovery of Zn using conventional hydrometallurgical processes (i.e., sulfuric acid leaching) is suitable, however the application of unconventional biohydrometallurgical techniques could be explored, as well re-smelting. These slag materials are classified geo-environmentally as potentially acid forming, with leachate concentrations of Zn, Pb consistently above ANZECC (2000) aquatic ecosystem 80% protection guideline values, and, for the majority of samples, exceedances of Cu, Ni and Cd were also measured. Considering these findings, reprocessing of these historic slags for Zn extraction may provide an economically feasible management option for rehabilitating this historical site.

Keywords: mineral processing; environmental management; acid and metalliferous drainage; mine waste; circular economy; waste valorisation

1. Introduction

Increasingly, questions are being posed regarding how the global community can sustainably support humanity's growing need for resources, and how waste created in the process should be handled [1]. Following detailed characterization, repurposing of waste could be a possibility in nearly every manufacturing sector, suggesting that a proportion of waste could be a potential resource [2,3].

This is significant for the mining industry because, globally, this sector is a major contributor to waste production, with at least 2.7 billion tons of mineral processing waste (e.g., waste rock, tailings, slag, spent heap leach) generated annually [4]. While there is a general trend of improved sustainable management in most modern mining operations (as stricter environmental guidelines and planning are in place [5]); issues still arise at historic and legacy mines or processing sites which contain mine and smelting waste. These present geo-environmental risks to the surrounding environment and can persist for decades, if not centuries, if not adequately rehabilitated. Ultimately, at mine-impacted sites, the source–pathway–receptor pollutant linkage chain needs to be broken [6]. Traditionally, this is performed reactively (i.e., with efforts concentrated on treating the pathway or receptor). However, adopting a more proactive management approach, aligning with the UN (2015) Sustainable Development Goals and Circular Economy principles [7] and based on mineralogical and chemical properties of the pollutant source material, may facilitate the development of an effective rehabilitation plan in which waste reprocessing may be a feasible option.

This study focusses on pyrometallurgical waste (i.e., waste products of ore smelting), commonly known as slag. The chemical and physical characteristics of slag are controlled by a wide range of factors including the type of ore processed, the metal (or metals) being targeted for extraction, the processing steps, the type and amount of fluxes added, the operating conditions of the furnace and the settling and cooling environment of the slag [8]. Consequently, slags tend to be compositionally and texturally heterogeneous and mineralogically diverse [9]. For this reason, the characteristics of slag cannot be extrapolated from one site to another, however, some commonalities between different sites have been observed, as summarised in [8,10]. Understanding the deportment of potentially deleterious elements within such complex materials is critical for defining the environmental risks posed by this metallurgical waste. Contaminant pathways can be aqueous, through percolation of water through waste piles and into surface and ground water, as well as airborne, through the weathering of slag piles generating dust [11]. An alternative approach is to consider historical slag as a potential resource. This concept has received increasing scientific interest since the 1990s. For example, slag materials have been used as construction materials, for metal recovery, in fertilisers and in environmental remediation projects [12,13]. The physical morphology of slag can make it useful as a raw material (e.g., road building, concrete aggregate, construction fill; [14]). Thus, whilst slag materials present environmental management challenges, they may harbor vast economic potential. The aim of this study was to determine the geometallurgical properties and geo-environmental risks posed by slag at the Zeehan historical smelter site located on the West coast of Tasmania, Australia. Slag was produced at this site in the late 1800s to 1910s. Such historic slags differ from their modern counterparts as they are characterised by elevated base metal and metalloid content, typically due to inefficient metal recovery technologies used at the time [9].

2. Site Description

2.1. Local Geology

Ore processed at Zeehan originated from mineral fields at Zeehan, Montana, Adelaide (replacement, vein and skarn deposits), Hercules and Rosebery (volcanic hosted massive sulfide deposits, [15]). These mines were targeted mainly for Pb and Ag, with minor Zn and Cu recovered where possible [15]. Mineralisation occurs in the Neoproterozoic Oonah Formation which comprises metapelites, carbonates, mafic volcanic rocks and occasional conglomerate units. The Oonah Formation is intruded by Devonian granitoids which are associated with vein and skarn type polymetallic (Pb, Zn, Sn, Ag) mineralisation dominated by galena (PbS), sphalerite ((Zn,Fe)S) and cassiterite (SnO_2) (Figure 1; [16–18]). Other mines in the area, such as Rosebery and Hercules, form part of the Cambrian Mount Read Volcanics, which hosts abundant polymetallic massive sulfide deposits containing Zn, Pb, Au, Ag and Cu [17,18].

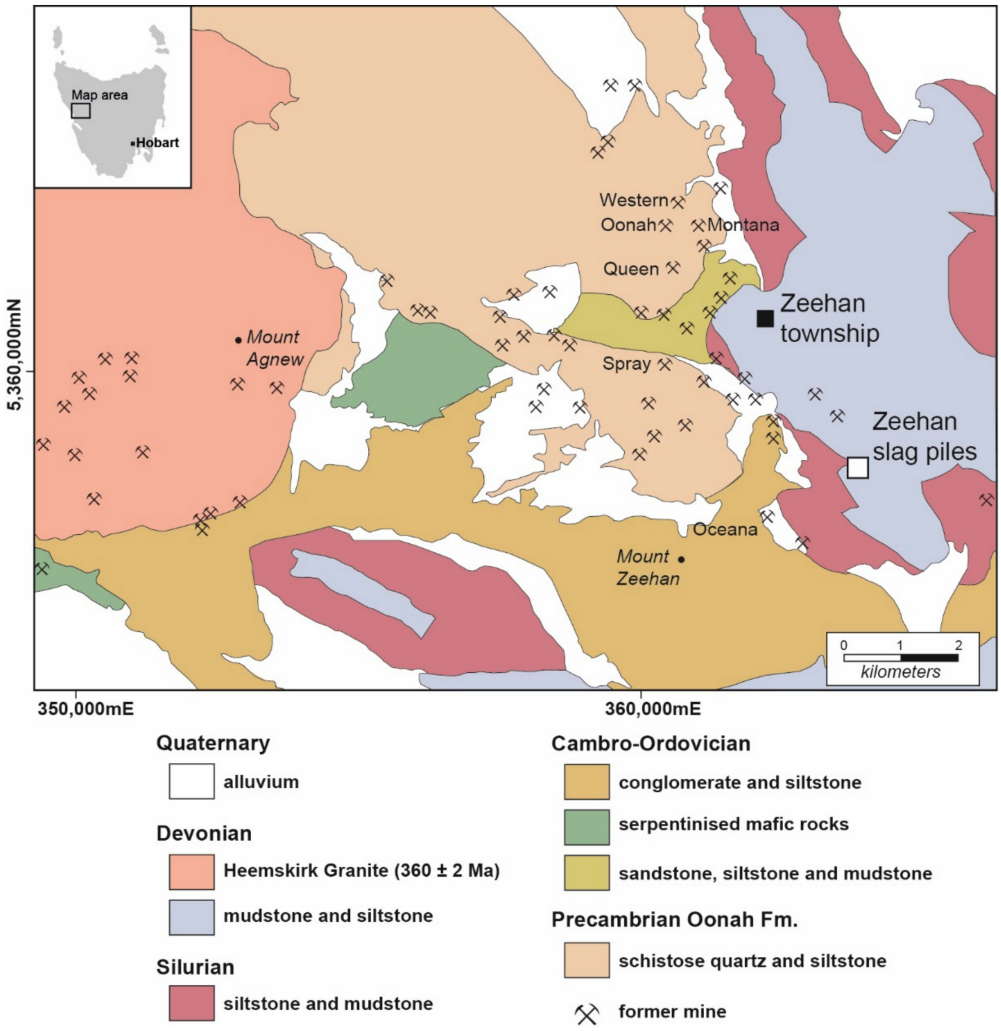

Figure 1. Geological map of the Zeehan field, Western Tasmania, with the location of the Zeehan slag piles and township marked (Modified from Fox et al. [19]).

2.2. Mineral Processing

Mining commenced in the 1880s at numerous sites including Spray, Oceana, Florence and Montana (Figure 1). Throughout the late 1800s and into the early 1900s, a localised mining boom was experienced, with Zeehan becoming a hotbed of investor activity, with new mining companies established, joint ventures set up and existing operators rebranding or expanding [15]. The Tasmanian Smelting Works, approximately 5 km south east of the Zeehan township, began operation in 1896 and processed Ag–Pb ores from the Zeehan fields. Originally, the smelting plant consisted of three blast furnaces with a daily capacity of 250 tons of ore, where two of the furnaces were used for Pb–Ag ore and the third for Cu ore from Rosebery, but this was later converted to a Pb furnace [20]. The smelter struggled to compete economically with European smelters for treating high-grade ores. It also faced difficulty in processing low-grade ores and was unable to efficiently separate Zn, which, with low metal prices, led to closure in 1909. Operations were able to resume two years later, but the works faced closure again in 1913. Finally, in 1923, a crushing and calcinating plant was built at the site, followed by a flotation plant, which were operational up until 1930, when low metal prices once again forced closure [15]. Engineering works to modify the plant and roasting mills started in 1931, and the refurbished plant operated from 1936 to 1948. The site has since been closed.

2.3. Site Description

The Zeehan slag piles are situated to the east of the Zeehan syncline and comprise the North and South slag piles (collectively, 469,000 t; 13.3% Zn, 1.7% Pb and 53 g/t of Ag). In addition, a tailings pile sits south of the South slag pile and ends at the bank of Austral Creek (Figures 2 and 3).

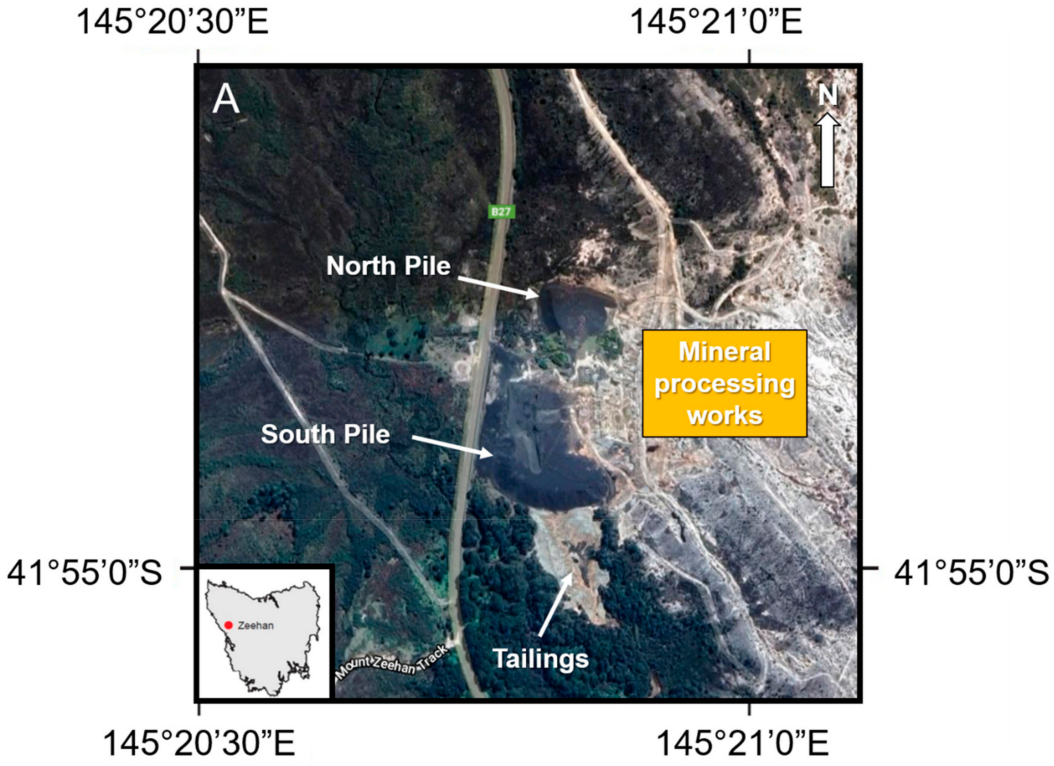

Figure 2. Mine waste features at Zeehan (map image from Google Earth).

The surface of the slag and tailings piles are uncovered, with only *juncus pallidus* (commonly observed at mine-impacted sites across Tasmania) present adjacent to surface channels where hardpan is also observed (Figure 3). The site experiences a cool temperate climate, with average rainfall of 402 mm and high rainfall during May to October, and with mean maximum temperatures around 15 °C (Supplementary Figure S1). The geology at the site comprises the Mt Zeehan Conglomerate, Moina Sandstone, Gordon Limestone and the Crotty Sandstone [21,22]. The Gordon Limestone sits directly below both slag piles, with surface outcrops of this unit hidden by them. The geo-environmental signatures of both mine waste types are distinctive, however, their relationship is influenced by the geology and climate, as described by Taylor [23]. He reported that the tailings intermittently discharge high concentrations of acid and metalliferous drainage (AMD), including Zn, As, Pb, Fe, Mn, Mg and V, with base flow mass loadings of up to 2 t/yr Zn, 48 kg/yr As, and 3 t/yr Fe. Surficially, the sulfidic tailings produce AMD, with pH measurements as low as pH 1.7 recorded. However, the underlying Gordon Limestone neutralizes AMD from the tailings during base flow discharge. Where surface water and ground/ creek water interact, precipitation of flocculants for those metals that have solubility particularly sensitive to pH changes (e.g., Al) occurs (Figure 3). While the AMD risk posed by the tailings is much greater than that of the slag [23], it is estimated that the slag piles contributes approximately 3.5 t/yr of S and 0.75 t/yr of Zn to Austral Creek.

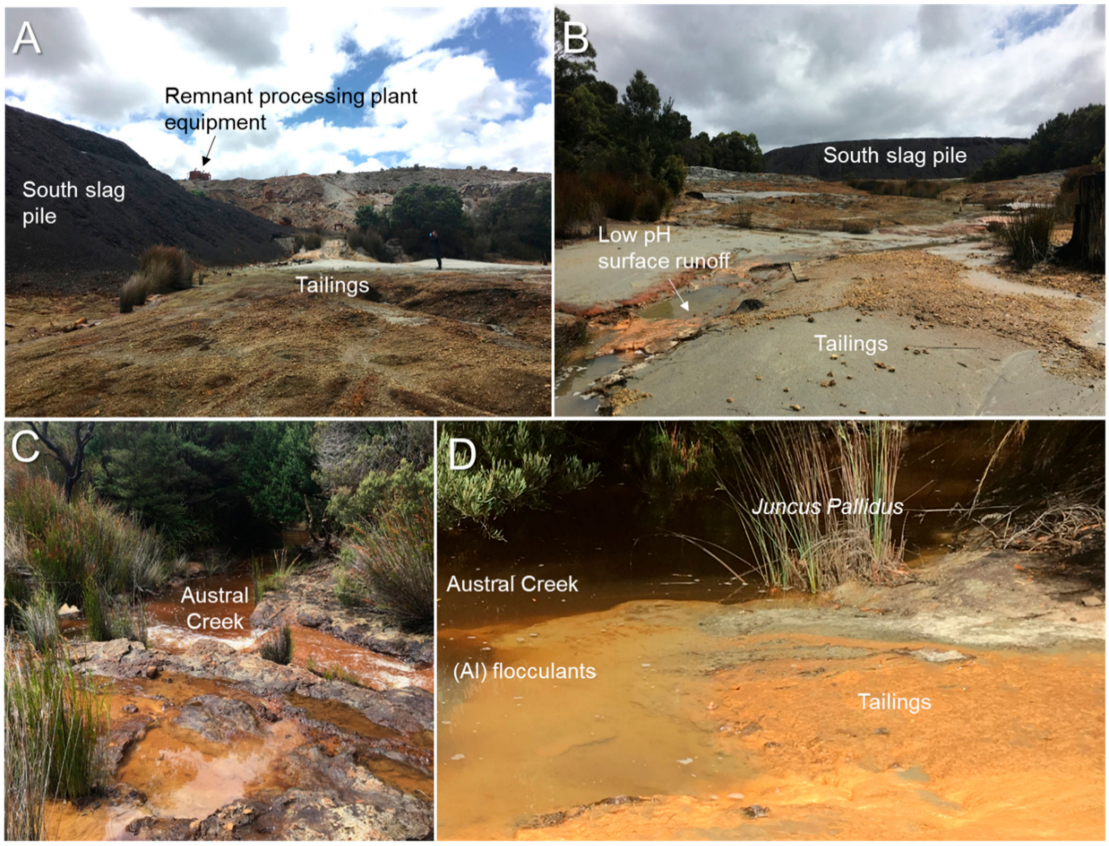

Figure 3. Images of slag and tailings mine waste at the Zeehan site: (**A**) Mineral processing equipment adjacent to the slag piles. (**B**) Uncovered tailings with localised surface water accumulation and hardpan. (**C**) Austral Creek at the very south of the tailings. (**D**) Precipitation of flocculants at the surface water–Austral Creek interface.

3. Materials and Methods

3.1. Sampling and Sample Preparation

Grab samples, comprising 5 to 15 cm^3 clasts, were taken from the top surface of both slag piles only, as this was safest to sample (i.e., plateaus with flat tops and steep slopes). Fourteen sampling cells were defined on each pile (8 m by 8 m gridded sampling cells covering the top of the North pile (the smaller of the two, example shown in Figure 4) and 15 m by 15 m sampling cells arranged on the South pile). As the piles were different sizes, the cells size also differed. Ten grab samples were randomly taken within each cell. The grab samples from the 24 cells (n = 280) were photographed, labelled and described with a macro-textural classification system devised using 10 defined classes (blocky, layered, vesicular, ropy, striated, metallic, pitted, smooth, acicular and granular). The grab samples from each cell were then composited to make 28 bulk samples from the two piles. Polished epoxy mounts (3 cm diameter) were prepared from each bulk sample for mineralogical and microtextural evaluations using secondary electron microscopy (SEM) and laser ablation inductively coupled plasma mass spectrometry (LA-ICPMS). The remaining bulk composite samples were crushed and rotary split into eight equal fractions. A single 1/8 portion was selected for pulverising in a ring mill (chrome steel ring mill; *p80* of <75 µm) to be used for a range of static, chemical and mineralogical analyses.

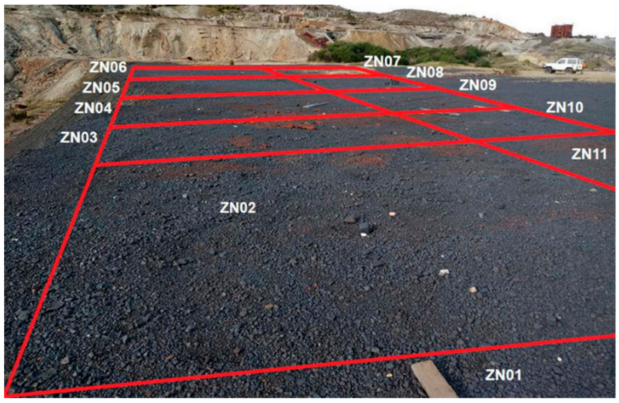

Figure 4. Example of sampling cell dimensions on the surface of the Zeehan North pile.

3.2. X-Ray Diffractometry

The bulk mineralogy of each quadrant was determined from the pulverised material using X-ray powder diffractometry (XRD) analysis. Each sample was spiked with approximately 10% by total sample mass of pure corundum powder and milled with an agate pestle and mortar to <10 µm prior to analysis. A benchtop Bruker D2 Phaser X-Ray diffractometer (Bruker AXS GmbH, Karsruhe, Germany), with a Co X-ray source, located at the Central Science Laboratory (CSL), University of Tasmania (UTAS), was used for the analysis. Each analysis was run for 1 h, using an operating voltage of 30 kV and current of 10 mA. Each scan ranged from 4° to 90° 2θ using a 0.02° 2θ step size, counting for 0.8 s per step. Mineral phases were identified using the Bruker DIFFRAC.EVA software package (Version 3.0, Bruker AXS, GmbH, Karsruhe, Germany), and the mineral database used was the PDF-2 powder diffraction file (2012 release). TOPAS (V.4.1) pattern analysis software (Bruker AXS GmbH, Karsruhe, Germany) was used to semi-quantify mineral abundances using Rietveld analysis. Due to the highly amorphous nature of phases in the sampled slag (estimated to be between 35 to 70% in Zeehan) the XRD results have been used for semi-quantitative mineral identification (i.e., taken as relative indicators only).

3.3. Bulk Chemistry

A portion of each powdered sample was analysed by Australian Laboratory Services (ALS) to determine the whole rock chemical composition using method code ME-MS61L. Samples were digested using a four-acid digest comprising additions of nitric, perchloric, hydrofluoric and hydrochloric acids. Aliquots were then analysed by inductively-coupled plasma atomic emission spectroscopy, inductively-coupled plasma mass spectrometry (ICP-AES and ICP-MS) for major and trace elements; a 25 g split of pulverised material was analysed by fire assay and atomic absorption spectroscopy (AAS) using method code Au-AA25. To enable determination of maximum potential acidity (MPA), total sulfur (in addition to nitrogen, hydrogen and carbon; all in %) was measured using a Thermo Finnigan EA 1112 series flash elemental analyser at the CSL. The samples were weighed (approx. 500 mg) using a Sartorius Microbalance SE2, a high precision balance with a readability of 0.1 µg. The results were calculated against the initial weight to get the percentage of the measured elements.

3.4. Static and Leach Testing

3.4.1. Soluble Metals

As surface salts were identified at the site on the surface of the piles (e.g., goslarite; Figure 5) it was considered necessary to quantify which metals may be easily leachable in a rainfall event (following a period of dry weather). Paste pH tests are fast, simplistic methods for determining the available acidity and salinity in such samples, and can also be used to determine the water soluble or exchangeable

fraction of elements [24,25]. The method used in this study is the procedure outlined in the AMIRA P387A Handbook [26]. It uses a 1:2 (25 g/50 mL) ratio of solid material to deionised water. This is left resting for 24 h to equilibrate the sample and the deionised water. The pH and EC (electrical conductivity) were measured in triplicate with the results averaged. In this study, the standard deviation for the triplicates was <0.05. Blanks (n = 2) consisting of 50 mL of deionised water were also measured in triplicate for pH and EC. After each measurement, 5 mL of the paste slurries and blanks was extracted using a clean syringe, filtered (0.45 µm PES Millipore) and preserved with a few of drops of 1% HNO_3 prior to solution ICP-MS analysis to identify the water-soluble elements and their relative proportions.

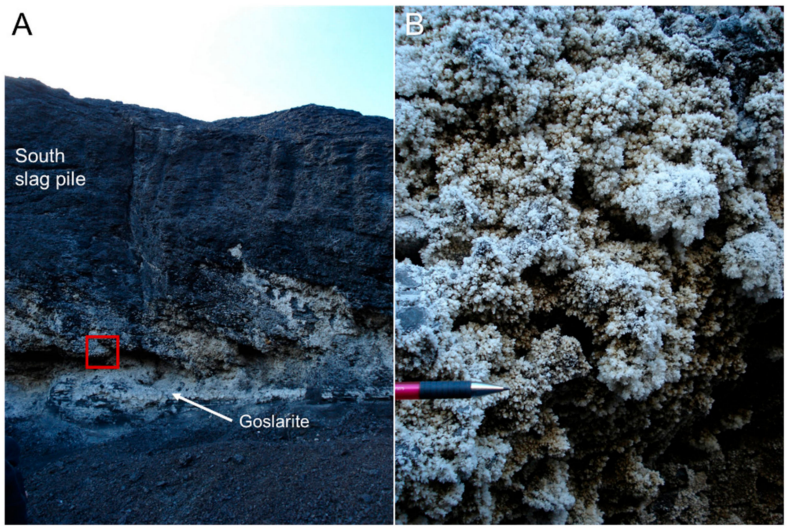

Figure 5. Zeehan south slag pile with: (**A**) Goslarite ($ZnSO_4{\cdot}7H_2O$) seen at the base; (**B**) Close up of white goslarite crystals.

3.4.2. Sulfide Oxidizable Fraction

Variable quantities of sulfides likely undergoing oxidation are contained in the slag materials in both piles [23]. To quantify the metal load contributed by this process (therefore enabling geo-environmental classification) net acid generation (NAG) pH testing was performed. Specifically, the multi-addition NAG pH test used on mine waste or processing residues was performed, which involves the addition of a hydrogen peroxide (H_2O_2) solution to the sample. It is used exclusively when samples contain high sulfur (i.e., >0.3% [27]), and benefits from a longer reaction time. The multi-addition NAG procedure used was adapted from the AMIRA P387A Handbook [26], with 30% strength H_2O_2 used instead of the recommended 15% to encourage total sulfide oxidation [28]. The pH and EC measurements were taken in triplicate, with duplicate samples analysed with the standard deviation calculated as <0.03. The leachate from each sample (60 mL) was collected using a syringe for solution ICP-MS, passed through a 0.45 µm mesh PES Millipore filter and preserved with 2 mL of 1% HNO_3.

3.4.3. Solution ICP-MS

The filtered and preserved leachates, comprising paste and NAG leachates (n = 56), blank standards (n = 2), random sample triplicates (n = 4) and random indium spiked samples (n = 6), were analysed by solution ICP-MS using an Element 2 HR-ICP-MS instrument at the CSL, UTAS. Calibration standards were made using single and multi-element analytical solutions. The major element standards (K, Fe, Al, Na, Ca, Mn and Pb) were made up to 10, 50, 100 and 10,000 ppb. Trace element standards were made up to 10, 100, 200 and 1000 ppb. Internal standards 115In (5 ppm) and 185Re (5 ppm) were used and added inline. The data were processed using proprietary instrument software (ThermoFisher, Waltham, MA, USA).

3.5. Microscopy

An automated Nikon Eclipse LV100 microscope with DS-Ri2 imaging attachment (Nikon Instruments, Tokyo, Japan) was used with Prior Proscan III for automation and NIS-Element AR 4.6 software (Nikon Instruments, Tokyo, Japan) for reflected light analysis of the polished block samples. The 10× nosepiece was used for imaging, with 3 × 8 bit 1608 × 1608 resolution and 10% overlap to capture 100 µm wide strips for the length of each laser mount. Based on the results, select samples were texturally examined further using a Hitachi SU-70 analytical field emission scanning electron microscope (FE-SEM) at the CSL. Samples (n = 17) were carbon coated prior to analysis and analysed using a current and voltage of 17 kV and 24 eV, respectively, in back-scattered electron mode. Data were acquired and processed using Oxford AZtec software (v.2.3, Oxford Instruments NanoAnalysis, High Wickham, UK) at the CSL. Mineral identification was determined with the assistance of Micronex MinIdent-Win 4 (v.3.3, Micronex, Edmonton, AB, Canada).

3.6. Laser Ablation ICPMS

Mineral identification (silicates vs. sulfides) was undertaken prior to LA-ICPMS, as described in the previous section. Spot analyses (n = 461) were performed on selected samples (n = 15) using a Resonetics Resolution 193 nm Excimer laser coupled to an Agilent 7700 ICPMS at the Centre for Ore Deposit and Earth Sciences (CODES) Analytical Laboratories. Calibration was performed using the standards NIST612, BCR-2G and GSD-1G (internationally recognised standards), and in-house sulfide-rich glass STDGL3 (internally prepared CODES lithium borate sulfide-rich glass). These were analysed between the spots at nine intervals to measure background levels (30 second background run; 60 second analysis). Silicate and glass phases were analysed with a 30 µm beam at 5 Hz and a fluence of 3.5 J/cm^2. Sulfide and oxide phases used a 19 µm beam at 5 Hz and a fluence of 2.7 J/cm^2. Each laser spot location was pre-ablated with five shots to clean the surface, and then for a further 60 s of analysis time, with a total of 43 elements measured. LA-ICPMS mineral analyses were processed using the newly-developed LADR software (1.0.8.0, Norris Scientific, Hobart, Australia) [29]. Using this new software, LA-ICPMS analysis does not necessarily require the direct measurement of an internal standard element by electron microprobe (c.f., Schindler, [30]). Major element Fe was selected as the internal standard during the quantification setup, as it is common to all silicate, oxide, and sulfide phases analysed. From the resulting time-resolved data for each analysis, homogeneity of Fe was assessed, and observed to behave in a manner reflecting homogeneous distribution in the mineral phase (i.e., patterns were smooth and not spiky as for element inclusions, see Supplementary Figure S2 for an example spectrum). For silicates, results were normalised to 100% oxide components. For sulfides, results were normalised to 100% sulfides, assuming mono-sulfide (sphalerite) stoichiometry. From the normalised major components, mineral identification was verified against acceptable stoichiometric compositions, i.e., olivine, pyroxene, sphalerite, etc. Any analyses that did not meet the major element stoichiometric criteria were excluded from the dataset. Thus, only data from time periods where spectra produced "clean" mineral signals were used, while those with chaotic, mixed mineral or inclusion-rich signals were excluded. These data were interpreted using ioGAS software (v7, Imdex, Perth, Australia).

4. Results

4.1. Bulk Properties

The main mineral-like phases identified in the slag included several types of olivine, pyroxene, mellite, spinel, sulfide, oxide and glass. Both slag piles had the same major mineral phases (Figures 6 and 7), with amorphous glass phases dominating (South pile: 36.5 to 52. 9 wt. %; North pile: 49.1 to 62.2 wt. %) followed by monticellite–kirschsteinite series ($CaMgSiO_4$ to $CaFe^{2+}SiO_4$) phases (North pile: 22.4 to 22.5 wt. %; South pile: 22.3 to 22.5 wt. %). Other dominant phases included hardystonite ($Ca_2Zn(Si_2O_7)$), wüstite (FeO), wurtzite ((Zn,Fe)S) and petedunnite ($Ca(Zn,Mn,Mg,Fe)Si_2O_6$), with higher

proportions measured in the South pile (Figures 6 and 7). Excluding amorphous phases, approximately 26% (North pile) and 32% (South pile) of phases (i.e., wüstite, litharge, monticellite-kirschsteinite and hercynite) did not contain Zn in their crystal structure. However, this does not preclude them from being Zn hosts, as during pyrometallurgical processing, there is potential for Zn incorporation into the lattice, as described in References [8,31], where Zn substitution for Fe in olivine, spinel and pyroxene is reported.

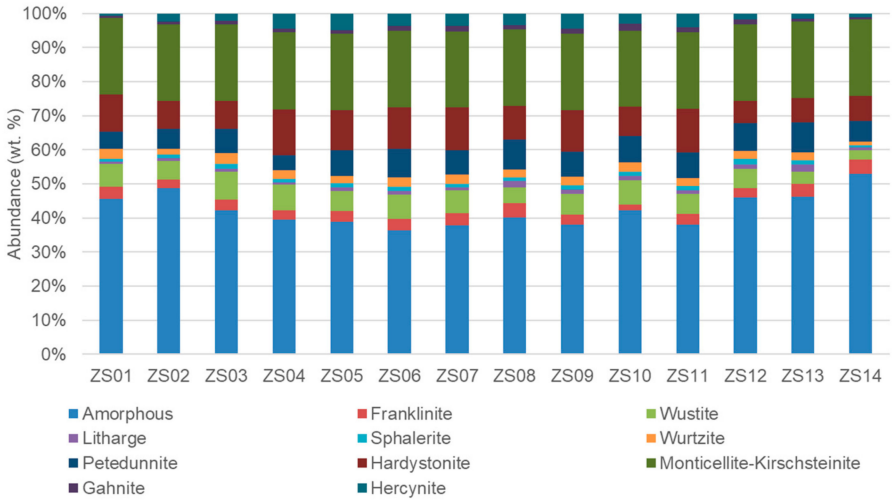

Figure 6. Abundance of the mineral-like phases identified in the Zeehan South pile (measured by X-ray diffraction (XRD); results are semi-quantitative).

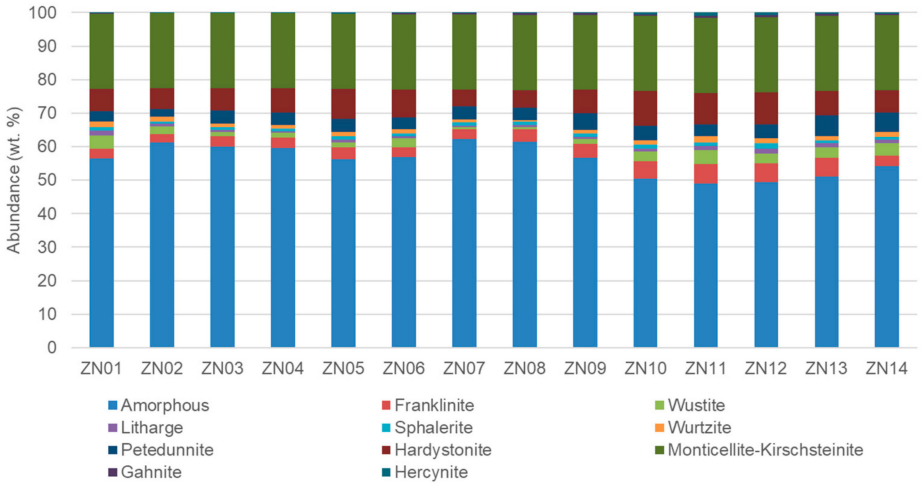

Figure 7. Abundance of the mineral-like phases identified in the Zeehan North pile (measured by XRD; results are semi-quantitative).

The average major element chemistry of both piles was similar, with (aside from O) Fe (21–26 wt. %), Zn (11.2–15 wt. %) and Ca (7.2–9.9 wt. %) the major constituents (Figure 8; Supplementary Table S1). The measured Zn concentrations are considered typical of blast furnace slag in the period prior to when Zn fuming was employed to enhance its recovery [32]. In comparison to other non-ferrous slag sites, a study of [33] the Hegeler Zn smelter, Illinois, America, identified a Zn-rich slag (with 28.4 wt. % Zn measured) amongst other slags where between 212 and 14,900 mg/kg was measured. Puziewicz et al. [34] studied the Świętochłowice dump in Upper Silesia, Poland, and similarly identified a Zn-rich slag (containing between 27 and 47 wt. % Zn, with willemite and zincite identified as host phases) amongst other weathered slags (2 to 5 wt. %). The measured Zn in the Zeehan slag was notably lower than the Zn-rich slags at Hegeler and Świętochłowice, though it is more homogenous in that

only one slag "type" was identified. However, it is important to reiterate that in this study, sampling was performed on the top surface of the pile (similar to Puziewicz et al. [34]); therefore, materials towards the bottom of the pile may show compositional variation, as observed at the Świętochłowice dumps (as reported in Tyszka et al. [35]).

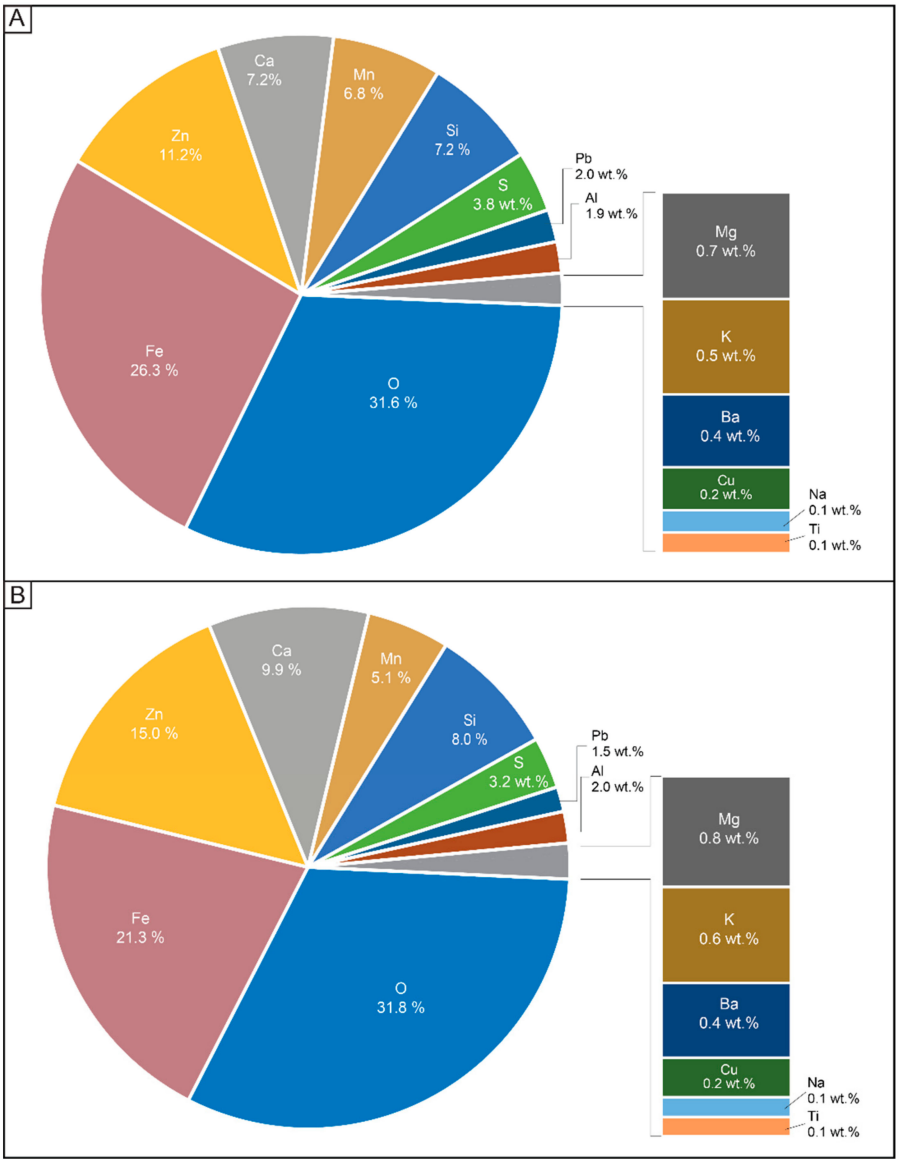

Figure 8. Element (wt. %) abundance from whole rock analysis inductively-coupled plasma mass spectrometry (ICP-MS) and inductively-coupled plasma atomic emission spectroscopy (ICP-AES) based on location: (**A**) North pile and (**B**) South pile.

The average Pb and Cu contents in both piles were 1.5 to 2% and 0.2%, respectively (Figure 8, Supplementary Table S1), which, for both elements, is greater than values reported for the Hegeler and Świętochłowice sites, potentially reflecting a cumulative effect of higher ore grades and comparatively less efficient processing in Zeehan. Further, remnant Ag was identified at Zeehan (North pile average: 82 mg/kg; South pile average: 52 mg/kg). Elements of environmental interest included As (North pile average: 416 mg/kg, South pile average: 384 mg/kg), with these values much lower than concentrations of 200 to 1900 mg/kg reported by Tyszka et al. [35], though Zeehan exceeded those measured at Hegeler (45 mg/kg). In contrast to Świętochłowice and Hegeler, Cd was not a contaminant of concern at Zeehan, with <10 mg/kg measured in both piles. Cobalt (North pile average: 49 mg/kg; South pile average:

31 mg/kg) and Ni (North pile average: 106 mg/kg; South pile average: 63 mg/kg) were also lower than those reported at Hegeler (Co: 103 mg/kg; Ni: 711 mg/kg).

4.2. Geo-Environmental Classification

The total sulfur quantities for the North and South Zeehan piles ranged between 2.7 and 4.8 wt. %, with a corresponding maximum potential acidity (MPA) range of 83 to 146 kg H_2SO_4/t. Geochemical plots of paste pH and NAG pH versus total sulfur show that all the samples fell into the potential acid forming (PAF) field (Figure 9). Measured NAG pH values were only slightly more acidic (range: pH 5.19 to 6.03; average: 5.61) than paste pH (range: pH 5.38 to 6.68; average: 6.17), but were much higher than expected when considering their sulfur content. This likely reflects that the dominant sulfides, sphalerite and wurzite, typically produce a NAG pH value > 4.5 [36]. Lahiri and Sengupta [37] described that Fe-spinels (i.e., franklinite, as identified in these materials) can act as catalysts for H_2O_2 decomposition, thus serving to increase the final measured NAG pH value. Reference [26] also reported that elevated levels of Cu can cause rapid H_2O_2 decomposition, and, in these samples, the measured content of Cu (1.5 to 2%) was also likely to have affected H_2O_2 reactivity. Finally, reflected light images showed some sulfides were <63 µm (i.e., the grind size used during sample preparation), and therefore may not have reacted during the chemical experiments.

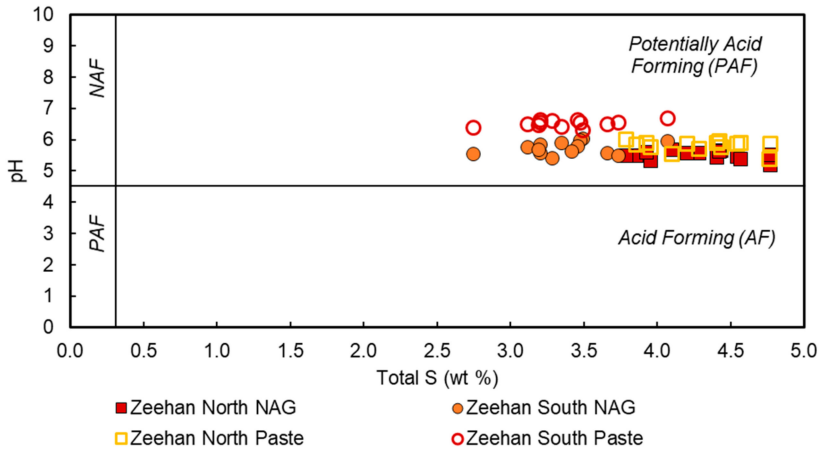

Figure 9. Classification of acid forming potential for bulk composites from the Zeehan North and South piles based on paste and net acid generation (NAG) pH versus total sulfur (wt. %). Abbreviations: AF—acid forming; NAF—not acid forming; PAF—potentially acid forming.

A Ficklin plot, commonly used as a geochemical assessment tool [38], is shown in Figure 10 for these data, with total elements (sum of Zn, Pb, Cd, Co, Ni and Cu in mg/L) shown against paste and NAG pH values. Using paste pH values, the majority of samples (86%) from both South and North piles classified near neutral–high metal, however, when plotted against NAG pH values, they classified in the near-neutral extreme-metal field. Interrogation of the geochemical data (Supplementary Table S2) demonstrated that Zn was the most abundant element (by one or two orders of magnitude) in the leachates when both deionised water and H_2O_2 were used as the extractants. However, on average, values were lower for the South pile (H_2O_2: 302 mg/L; water: 1.8 mg/L) than the North (H_2O_2: 581 mg/L; water: 2.9 mg/L). The next most abundant metal was Pb (H_2O_2: 0.9 mg/L to 1.9 mg/L in the South and North piles, respectively; water: 0.3 mg/L to 0.9 mg/L in South and North piles, respectively). For Zn and Pb, measured values were in excess of the ANZECC (2000) aquatic ecosystem 80% protection guideline values [39] (0.031 mg/L and 0.009 mg/L, respectively). With a deionised water extractant, the majority of samples also exceeded the ANZECC (2000) 80% protection guideline values for Cu, Ni and Cd of 0.0025 mg/L, 0.017 mg/L and 0.0008 mg/L, respectively [39].

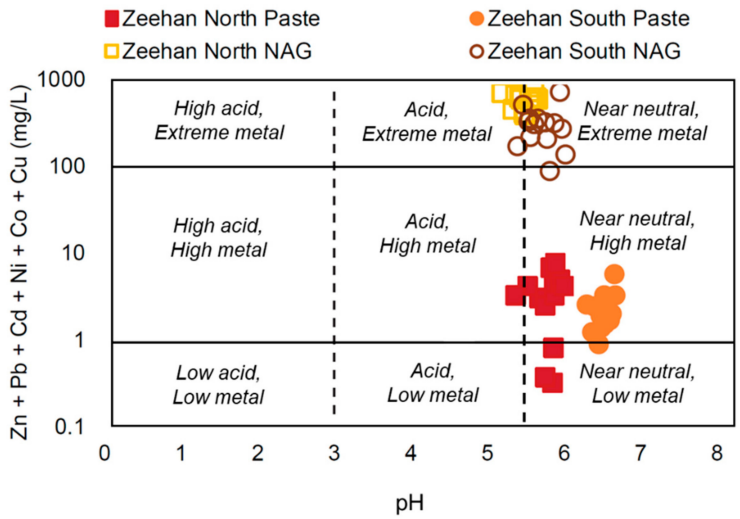

Figure 10. Ficklin plot [40] showing metals (mg/L) versus NAG pH and paste pH for Zeehan North pile and Zeehan South pile samples.

4.3. Microtextures

To better identify the mineralogical hosts of the environmental and economic elements of interest, the microtextures of the Zeehan samples were studied. In general, the slag demonstrated extreme micro-textural heterogeneity, reflecting differing cooling rates, however there were likely secondary influences too from the compositional differences of the smelted materials (sourced from different deposits in the mineral field) and the evolving smelting technology itself over the 40 years period. In general, microlitic, dendritic, porphyitic and spinifex textures were all observed in both piles. Glass dominated on the edges of the slag where it formed a rim, and became coarser towards the core of the sample (Figure 11A). Dendrites, a common texture in air-cooled slags, ranged from <5 µm to >300 µm in size and were observed in all analysed samples. The shapes varied from large elongated dendrites with well-defined branches to short poorly formed sub-dendritic networks (Figure 11B). Also observed were large prills of lead oxide, with approximately 50% of those observed appearing to have partially weathered on their rim (possibly to anglesite). Based on the average size of the observed dendrites, it is likely the slag cooled at a moderate rate, though the chemical composition may have also had an influence on their morphology [41,42]. In the porphyrtic textural class, euhedral to subhedral phases in a fine-grained groundmass were widespread and ranged from <5 µm to >2 mm in size. They ranged from tabular to rhomboidal in shape (Figure 11C), however, in the case of smaller phases, the boundaries were not visible, due to the presence of cross-cutting dendrites. Crystal growth can be random or directional, with some samples resembling large-scale spinifex textures or banding; tabular crystals can also grow perpendicular to the rims. Lath-like phases (Figure 11D) were observed in fewer samples and had a similar size range to the euhedral phases, but demonstrated more directional growth patterns. In this study, spinifex texture describes a very fine micro-scale texture (<10 µm across) infrequently seen (10% of samples; Figure 11E). Occasionally, large olivine phases containing lead oxide prills were observed in a microlite groundmass (Figure 11F).

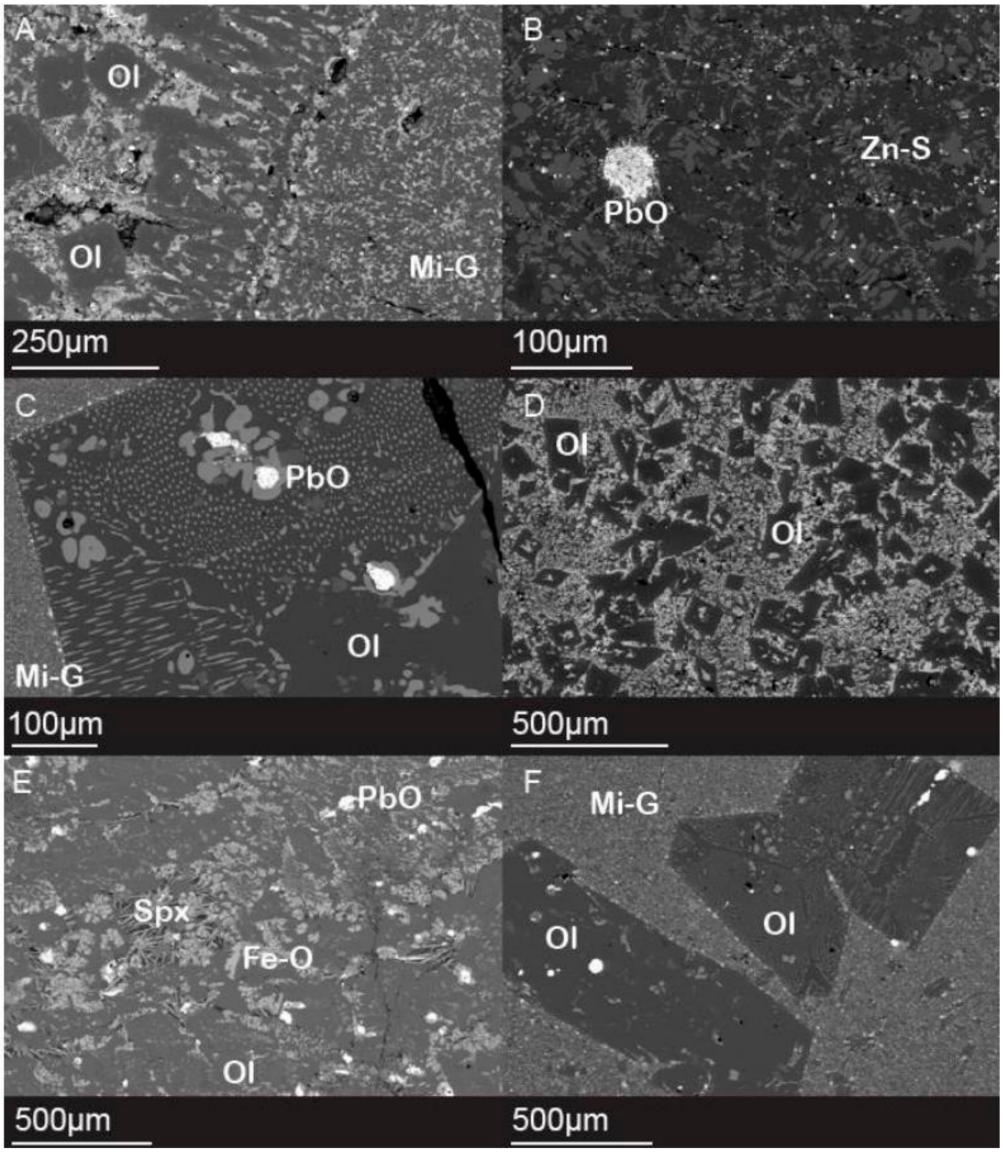

Figure 11. Backscattered scanning electron (BSE) images of polished epoxy mounts of slag from Zeehan. (**A**) Olivine in a microlitic groundmass (Fe oxide and Zn sulfide dendrites and Pb oxide prills) with euhedral spinels (ZN1408). (**B**) Pb oxide inclusion within wurtzite dendrites (ZN1404). (**C**) Centre of a clinopyroxene crystal, with a hopper texture (ZS0801). (**D**) Olivine micro-phenocrysts in a microlite groundmass (ZS1201). (**E**) Bands of olivine and dendrites with spinifex textured areas (black with light grey needles) throughout (ZS1306). (**F**) Olivine crystals with both plain and hopper textures, surrounded by a microlite groundmass (ZS0801). Abbreviations: Ol (olivine), Mi-G (microlite groundmass), PbO (lead oxide), Zn–S (zinc sulfide), Spx (spinifex texture) and Fe–O (iron oxide).

4.4. Mineral Chemistry

Following micro-textural evaluations, chemical analysis of the dominant mineral phases identified (i.e., glass, silicates, sulfides and oxides) was performed using LA-ICPMS. Nine mineral-like phases were identified, and, based on their mineral chemistry, the mineral they most resembled was determined as shown in Table 1. The characteristics of each mineral-like phase are described in the following section.

Table 1. Phase descriptions based on laser ablation inductively coupled plasma mass spectrometry (LA-ICPMS) data, showing class, phase name, its mineral resemblance (chemically) where appropriate and the chemical formula of named mineral. * Mineral compositional formula (for amorphous phases, this is an approximation based on elemental abundances from LA-ICPMS data).

Phase	Texture	Mineral Resemblance	Chemical Formula *
Glass A	Microlitic	Fayalite–Tephroite series	Fe_2SiO_4 to Mn_2SiO_4
Silicate A	Skeletal laths to euhedral crystals	Petedunnite	$Ca(Zn,Mn,Mg,Fe)Si_2O_6$
Silicate B	Skeletal laths to euhedral crystals	Fayalite–Tephroite Series/Kirschsteinite	Fe_2SiO_4 to Mn_2SiO_4/$CaFeSiO_4$
Silicate C	Skeletal laths to euhedral crystals	Kirschsteinite	$CaFeSiO_4$
Silicate D	Skeletal laths to euhedral crystals	Fayalite	Fe_2SiO_4
Sulfide A	Dendritic	Sphalerite and Wurtzite	(Zn,Fe)S
Sulfide B	Bleb contained in skeletal laths to euhedral crystals	Galena	PbS
Oxide A	Dendritic	Franklinite and Magnetite	$ZnFe_2O_4$ and Fe_3O_4
Oxide B	Bleb	Litharge, Massicot	PbO

4.4.1. Glass and Silicates

Glass A comprised Si, Fe, O, Ca, Mn (average = 8.3 wt. % Si; 17.2 wt. % Fe; 28.2 wt. % O, 9.1 wt. % Ca; 5.0 wt. % Mn) and Zn (average: 25.2 wt. %), and compositionally resembled olivine (fayalite–tephroite series). The composition of Silicate A (mean composition = 0.1 wt. % Na; 17.3 wt. % Ca; 1.5 wt. % Mg; 3.8 wt. % Mn; 15.5 wt. % Zn; 14.3 wt. % Fe; 12.7 wt. % Si; 32.4 wt. % O) most closely resembled petedunnite ($Ca(Zn,Mn^{2+},Mg,Fe^{2+})Si_2O_6$), a rare member of the clinopyroxene group (stoichiometric composition = 0.9 wt. % Na; 14.6 wt. % Ca; 1 wt. % Mg; 4.5 wt. % Mn; 10.6 wt. % Zn; 6.8 wt. % Fe; 22.8 wt. % Si; 38.9 wt. % O). The major difference between the stoichiometric petedunnite is the lower abundance of Si in Silicate A, which may be due to the slag melt being Si-poor [42]. Silicate B sat between the fayalite–tephroite series and the kirschsteinite–monticellite series. The concentration of Ca was too high for true fayalite (mean = 7.7 wt. % Ca), and both Fe and Mn concentrations were too high for kirschsteinite (mean = 24.3 wt. % Fe; 9.2 wt. % Mn). However, Si and O concentrations (mean = 11.8 wt. % Si; 30.9 wt. % O) were within the range for both series. Although the Fe concentrations were low for fayalite, this could be due to substitution of Zn for Fe in the crystal lattice [43]. Silicate C had the highest Mg and Ca values of the olivine phases (mean = 3.1 wt. % Mg; 20.5 wt. % Ca), and similar levels of Si and Mn (mean = 8.2 wt. % Si; 13.2 wt. % Mn) to the other olivine phases. It had the lowest concentrations of Zn and Fe (mean = 5.9 wt. % Zn; 14.0 wt. % Fe) and had the most similar composition to the kirschsteinite–monticellite series of all the silicates (kirschsteinite stoichiometric composition = 21.3 wt. % Ca; 29.7 wt. % Fe; 14.9 wt. % Si; 34 wt. % O). Silicate D most closely resembled fayalite (stoichiometric composition = 54.8 wt. % Fe; 13.8 wt. % Si; 31.4 wt. % O) with similar Si and O proportions (mean = 11.1 wt. % Si; 29.8 wt. % O). It had the highest concentrations of Fe, Mn, Zn and Al (mean = 27.9 wt. % Fe; 13.2 Mn wt. %; 14.1 wt. % Zn; 1.2 wt. % Al) in the olivines, and the lowest concentrations of Ca (mean = 0.6 wt. % Ca). The low Fe levels compared to fayalite may be explained through Al and Zn substituting for Fe in this phase [44].

4.4.2. Sulfides

Two sulfide phases were identified and classified as Sulfides A and B (Table 1). Sulfide A had dendritic textures, whereas Sulfide B referred to the prills/bleb shaped inclusions. The dendritic sulfides were one of two dendrite textures present in the slag. They were larger than the Oxide A

dendrites, with elongated, well-defined branches that formed various shapes, including X-shapes and rings. Sulfide A was dull grey in reflected light, but occasionally could appear iridescent. Chemically, it resembled a Zn–Fe sulfide such as wurtzite or sphalerite (wurtzite stoichiometric composition: 60.9 wt. % Zn; 5.8 wt. % Fe; 33.2 wt. % S). It, however, had higher Fe and S and significantly lower Zn (28.1 wt. % Zn; 13.3 wt. % Fe; 43.3 wt. % S). The higher Fe and lower Zn concentrations had the opposite trend to the silicate phase compositions, suggesting that the silicates may have formed before the sulfides causing Zn deficiency. Textural evidence supports this proposed paragenesis, with silicates demonstrating crystalline structures requiring more time to form than the dendritic textures of Sulfide A that likely formed from high temperature, rapid cooling environments [41]. Sulfide B resembled galena (stoichiometric composition = 86.6 wt. % Pb; 13.4 wt. % S) but a wide range of elements were also reported (e.g., Si, Fe, O, S, Cu, Zn and Pb) and likely were forming on secondary rim phases.

4.4.3. Oxides

The two oxide phases, A and B, differed chemically and texturally. Oxide A was typically smaller (<5 μm to >100 μm) than Sulfide A phase and was more poorly formed. They had the highest concentration of Fe of all the phases (61.7 wt. % Fe; 8.7 wt. % Mn; 5.6 wt. % Zn; 22.6 wt. % O), and most closely resembled franklinite (37.8 wt. % Fe; 9.0 wt. % Mn; 16.6 wt. % Zn; 27.1 wt. % O). Oxide B (83.1 wt. % Pb; 7.9 wt. % O) closely resembled litharge/massicot (92.8 wt. % Pb; 7.1 wt. % O), and was also present as prill/bleb like inclusions ranging in size from <10 μm up to >250 μm, but was less common when compared to Sulfide B.

4.4.4. Element Deportment

Several potentially economic (i.e., Zn, Pb, Ag, Cu) and environmental (i.e., As, Cd) elements were identified, but to determine which mineral phases contained them, LA-ICPMS results were further interrogated. The mineral-like phases containing the highest Zn were Sulfide A (average: 26.5 wt. %; Supplementary Table S3) and Glass A (average: 24.9 wt. %; Supplementary Table S3; Figure 12A). Whilst these measurements were high, they were lower than those reported at Świętochłowice, where Zn-rich oxide and silicate phases contained 27 to 47 wt. % of the identified silicate phases. The greatest Zn was measured in Silicate A (petedunnite; average 14.3 wt. %), which was slightly elevated in comparison to its stoichiometric quantity (10.6 wt. %; Supplementary Table S3). This was followed by Silicate D, a fayalite-like phase (average: 13.4 wt. %; Supplementary Table S3) which, Ettler et al. [45] report, is possible, as Zn can substitute for Fe in the *Y* position ($XYZO_4$, where *X* is a large cation, eight coordinated, *Y* is an intermediate-sized cation and *Z* a tetrahedral small-sized cation) during cooling. The mineral-like phase with the lowest measured Zn was Oxide B (average: 20 mg/kg; Supplementary Table S3).

Lead, a commodity once concentrated at the Zeehan smelter, was measured in seven mineral-like phases (measurements in Silicate B and Silicate C were below detection limits; Supplementary Table S3). Additionally, Glass A was likely devoid of Pb, as all but one of the measurements (8413 mg/kg) were also below detection limit. Where this was measured, it is postulated that Oxide B micro-inclusions are likely to have been analysed too in this spot (i.e., vertically underlying the analysed spot). Oxide B contained the highest Pb (Figure 12B, Supplementary Table S3) followed by Sulfide B (average: 24.6 wt. %; Supplementary Table S3) and Silicate A (average: 1.5 wt. %; Supplementary Table S3) where interrogation of LA-ICPMS data indicated Pb was present as microinclusions of Sulfide B and Oxide B. Typically, mineral phases high in Zn had lower abundance of Pb (e.g., Silicate Phases A to D; Sulfide A). This negative correlation can be explained by Zn and Fe minerals being poor hosts to Pb due to the large ionic size differences between Pb^{2+}, Zn^{2+} and Fe^{2+}, causing Pb to partition into coexisting phases (e.g., Oxide B and Sulfide A; Lockington et al. [46] observed the same phenomenon with Zn and Pb). Silver, another commodity recovered during metallurgical processing, was identified in all mineral-like phases (Figure 12C). Again, the highest measurements were made in Sulfide B (average: 292 mg/kg; Supplementary Table S3) and Oxide B (average: 127 mg/kg; Supplementary Table S3),

demonstrating association between Pb and Ag. This was followed by Silicate C (average: 140 mg/kg; Supplementary Table S3) and Glass A (63 mg/kg; Supplementary Table S3). The greatest concentrations of Cu were measured in Sulfide B (average: 8708 mg/kg; Figure 12D; Supplementary Table S3) followed by Glass A (average: 2424 mg/kg), with the lowest values reported from Oxide A (average: 2 mg/kg).

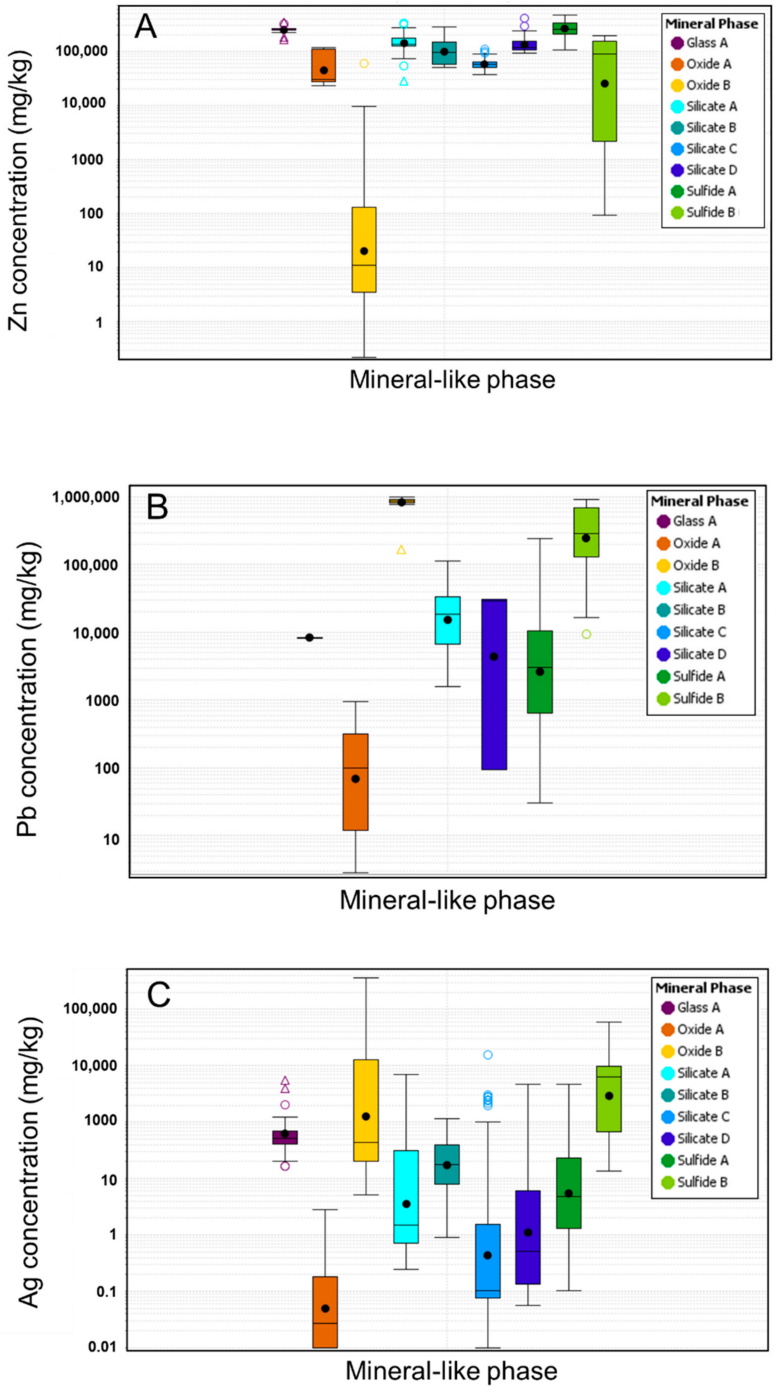

Figure 12. *Cont.*

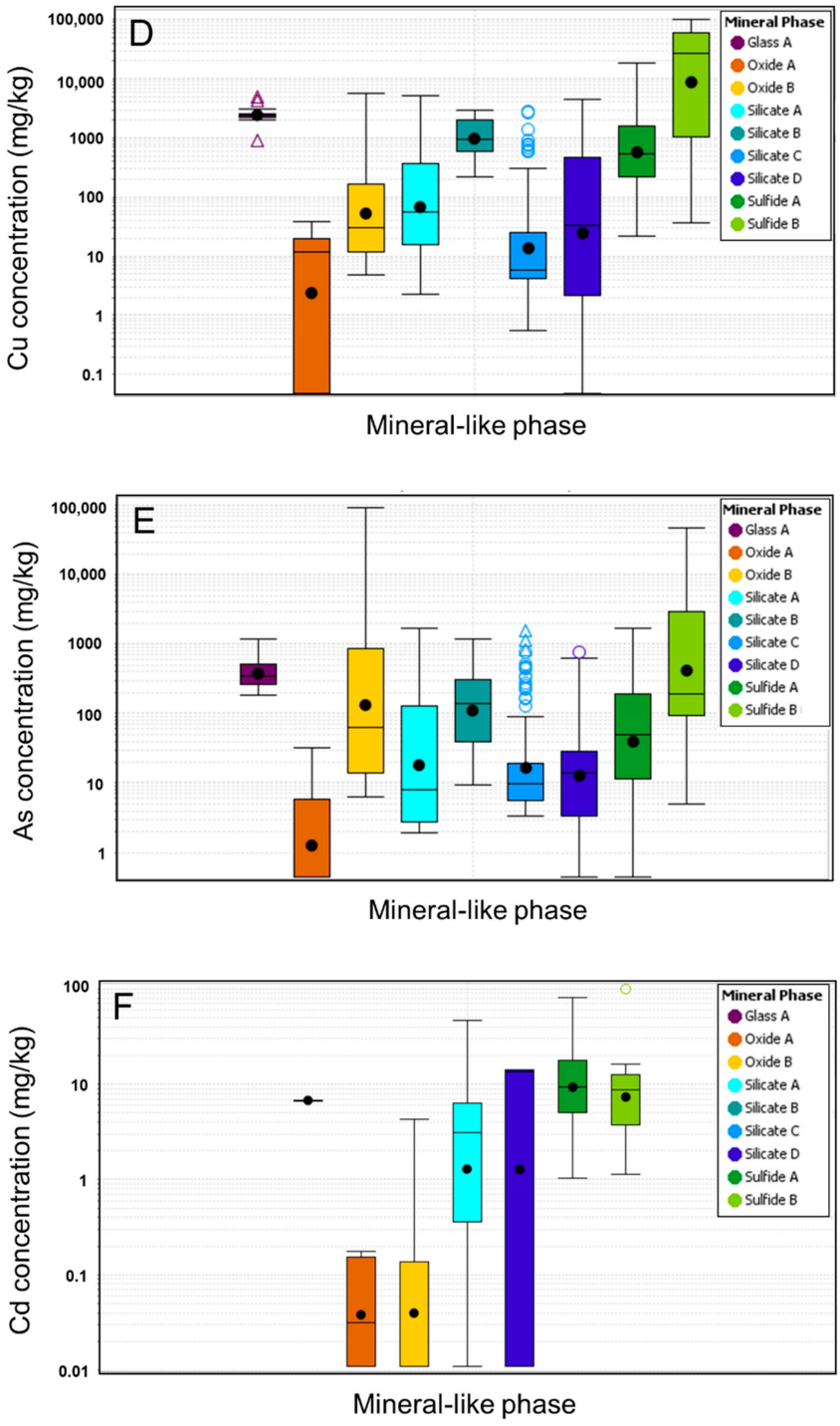

Figure 12. Box and whisker plot of economically significant element: (**A**) Zn, (**B**) Pb, (**C**) Ag and (**D**) Cu and environmentally significant element: (**E**) As and (**F**) Cd concentrations at Zeehan in the different mineral phases across both piles. Based on logged values, the top and bottom whiskers represent min and max for the phases, the top and bottom of the box representing Q3 and Q1, respectively, the black line is the median and the black circle is the mean of the logged values. The central box is the middle 50% of the data, outliers further than 1.5 from the box are represented by hollow circles, and outliers further than 3.0 are represented with hollow triangles. The whiskers are the extreme values that are not outliers.

A similar distribution of environmental (i.e., potentially deleterious) elements were observed, with the highest As measured in Sulfide B (average: 418 mg/kg) followed by Glass A (average: 377 mg/kg;

Figure 12E; Supplementary Table S3) and Oxide B (average: 132 mg/kg; Supplementary Table S3). Cadmium was not measured during the silicate and glass LA-ICPMS analysis. Instead, the highest Cd was measured in Sulfide A (9 mg/kg; Figure 12F) followed by Sulfide B (7 mg/kg; Figure 12F), with average contents in Oxides below 0.03 mg/kg; such values are regarded as low in comparison to Cd values reported at other sites (e.g., Lockington et al. [46] Tyszka et al. [47]). Compared to Cd, values of Ni and Co were much higher in all phases (Supplementary Table S3), with the highest Ni measured in Silicate D (89 mg/kg; Supplementary Table S3), and Co in Oxide A (118 mg/kg; Supplementary Table S3).

5. Discussion

5.1. Geo-Environmental Risks

Piatak et al. [8] reported that for non-ferrous slags which are (Fe) sulfide bearing, acid generation upon weathering is possible. Measurements in this study are in agreement with observations made by Taylor [23], who reported that water leaching from the slag piles had pH values between 3 to 4, with Sulfide A a likely source of acid and metalliferous drainage. While MPA values were 84 to 146 kg H_2SO_4/t, these slags also contained several olivine-like phases, which are considered acid neutralising [48]. However, their rate of dissolution is slow (compared to the acid generation from Sulfide A), and this diminishes their overall neutralising contribution [48]. Compared to other non-ferrous slag sites such as Rio Tinto, Spain [9], paste pH values at Zeehan were much higher (Zeehan: pH 5.38 to 6. 68; Rio Tinto: pH 3 to 5), suggesting these sulfides are not as reactive. Instead, Rio Tinto slags are dominated by Cu- and Fe-sulfides, which undergo oxidation quicker, therefore, the water quality risk posed by a Zn–Fe sulfide dominated site is considered lower.

While slag typically contains lower levels of potentially deleterious elements (e.g., Pb, Cu, Zn, and As) compared to other sulfidic mine wastes (i.e., tailings), they may still present risks that require management. The Zeehan smelter site is in close proximity to Austral Creek (a tributary to Little Henty Creek, which enters Trial Harbour). Meteoric water percolates through the slag piles, releasing constituents during weathering, which may eventually enter Austral Creek and the underlying groundwater [23]. Piatak et al. [8] presented a summary of leached elements versus total elements, however, the synthetic precipitation leaching procedure (SPLP) and toxicity characteristic leaching procedure (TCLP) values were used. In this study, 30% H_2O_2 and deionised water were instead used as extractants (and therefore are not directly comparable), so our values are instead screened against those published to indicate potential leachate quality issues which may require further detailed investigation. Zn in leachate (when using H_2O_2 as the extractant) was in the range of 87 to 795 mg/kg (deionised water results are less than 10 mg/kg with two distinct populations observed; Figure 13A), which is similar to concentrations measured for TCLP extracted metals in Pb and Cu slags [49] and Zn slags [33]. For Pb, leachate concentrations were considerably lower, with values below 2 mg/kg, and with values from the H_2O_2 extractant slightly higher overall (Figure 13B). These measured values are similar to those again reported for the Hegeler slag [33]. Copper values were most similar to Parsons et al. [49], and slag studied at the Vermont and Tennessee site studied by [50]. Leached Cd values were very low, with < 1 mg/kg measured from both extractants, with these values similar to Piatak et al. [50]. Arsenic in leachates was below instrument detection limit. While the comparison is general, the similarity of Zeehan slag to several different slags characterised by References [33,49,50] reflects that ores from several volcanic hosted massive sulfide and replacement type deposits were processed at the site. Despite their comparatively lower values (both in bulk and leachate chemical values) to these other non-ferrous sites, Zn, Pb, Cu and Cd values were in excess of ANZECC (2000) 80% aquatic protection guideline values [38]. Ultimately, the site's geochemistry is complicated by the presence of sulfidic tailings at the foot of the South pile (Figures 2 and 3), with the environmental risk posed by the slag piles considered to be lower, based on their characteristics reported in Taylor [23].

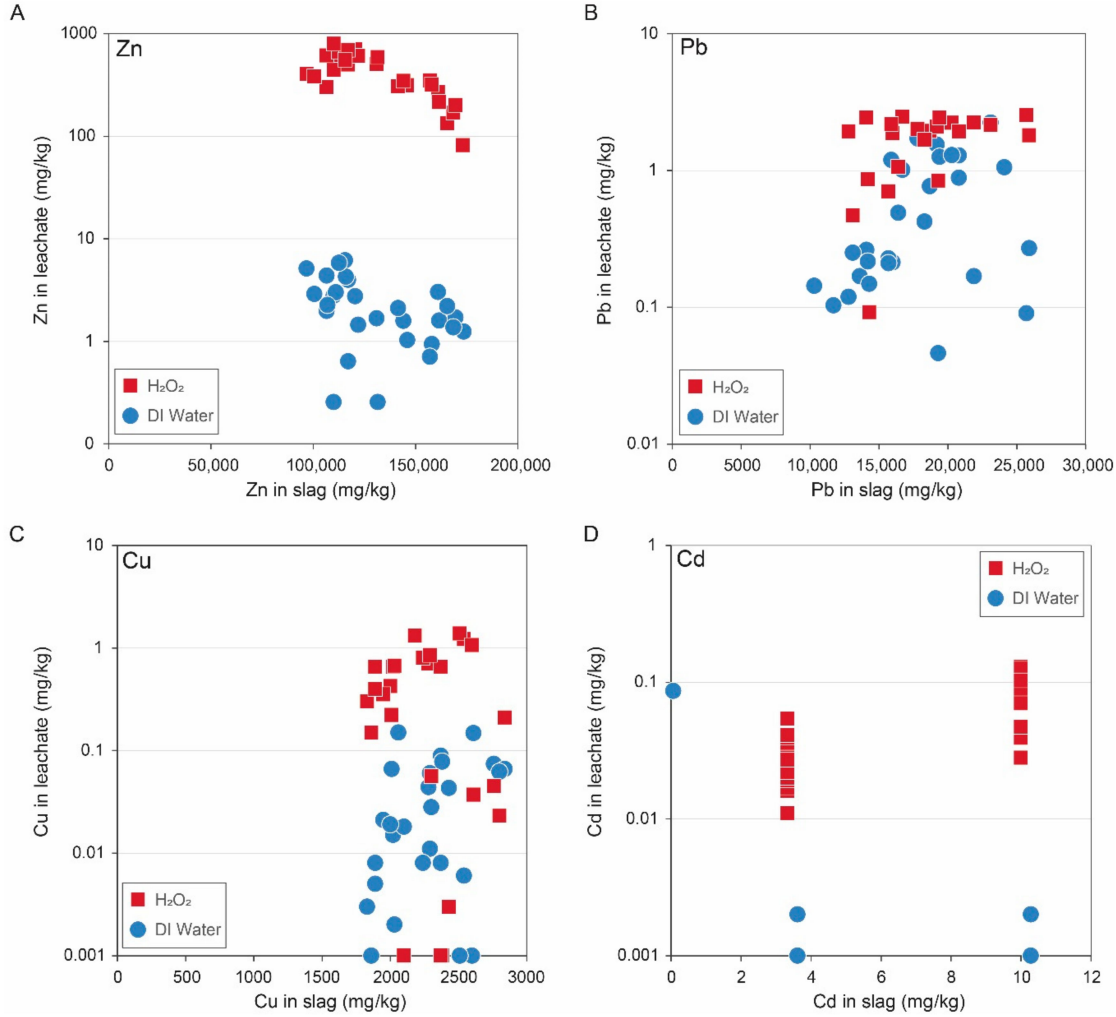

Figure 13. Chemistry of Zeehan slag leachates compared to concentrations of elements in the slag based on bulk chemical analysis for (**A**) Zn; (**B**) Pb; (**C**) Cu and (**D**) Cd. Concentrations are in mg/kg for both leachate and bulk chemistry; leachate concentrations were multiplied by the liquid-to-solid ratio to convert mg/L to mg/kg (DI water = deionised water; H_2O_2 = hydrogen peroxide).

Several recent studies have investigated the impact of dust dispersed from mine waste on the environment (e.g., References [51–53]). Prevailing wind controls the dominant direction of dispersal, with airborne pathways noted to facilitate greater distances to be travelled by potential contaminants when compared to waterborne pathways. While the prevailing wind direction near Zeehan is from the south-west, dust dispersal may pose a risk to the Zeehan community, which is just 5 km from the piles. With erosion and weathering processes occurring at the site since its establishment in 1896, the potential impact of dust from the site should be investigated.

5.2. Rehandling and Reprocessing Options

5.2.1. Chemical Reprocessing

While slag materials can be reused as construction materials [13], the Zeehan slag is an important secondary source of Zn, comparable to other early non-ferrous blast furnace slags, therefore, future activities at the site should focus on its extraction. The site is under a mining lease, with the owners investigating metallurgical options to monetize the Zn resource. Zinc deports to all mineral phases identified, with hydrometallurgical or pyrometallurgical processing options considered the most suitable. For example, the study performed by Kurama and Goektepe [54] focused on chemical

leaching of 300,000 t of slag to recover Zn and Fe from an abandoned Pb–Zn mine in Balya, Turkey. The Balya slag is of a similar age, size and composition to the Zeehan slag, with approximately 29% Fe, 13% Zn, 3% Pb and 2% S. The initial testing showed poor Zn extraction using low concentrations of H_2SO_4, which was attributed to high proportions of Zn being present as a ferrite (Zn–Fe_2O_4), which can be insoluble. The final recovery method involved a two-part extraction:

- Slag was initially subjected to leaching at 1.85 mol/L H_2SO_4 at 1/10 solid ratio at a temperature of 55 °C. The residue was then collected for a secondary leaching process.
- A concentrated solution of 4.07 mol/L H_2SO_4 was then added to the leachate at 1/10 solid ratio at a temperature of 95 °C to dissolve the ferrite phases. Ammonium jarosite was precipitated to recover any dissolved Fe.

This method resulted in the extraction of 77.4% Zn at atmospheric pressure, and 87% Zn using pressure leaching. The Zeehan slag has a phase resembling the Zn ferrite (Oxide A: Franklinite $ZnFe_2O_4$), which could cause comparable problems during reprocessing. Due to the similarities between the two sites and the successful metallurgical testwork at Balya, a similar methodology could be adapted for Zeehan. More recently, Ma et al. [55] investigated alternatives to using H_2SO_4 by using an alkaline leach (NH_3–CH_3COONH_4–H_2O) solution on a Zn-rich slag and dust composite (2–50 μm particle size). They reported that Zn extraction reached 83.7% when using a total ammonia concentration of 5 mol L^{-1}, stirring speed of 300 rpm, ammonia/ammonium ratio of 1:1 and solid/liquid ratio of 1: 5 for 60 min at 25 °C. However, if an alkaline leach was used at Zeehan, lower Zn recovery grades would be anticipated, as it was reported that Zn_2SiO_4, ZnS and $ZnFe_2O_4$ did not leach, suggesting that if this approach was used, Zn from Oxide A, Sulfide A and Silicate A (i.e., 44% of the contained Zn) might not be recovered. When considering 26% of Zn deports to Sulfide A and 24% to Glass A, both should ideally also be targeted during metallurgical processing. Management of Fe during processing will also be a key factor to consider. Typically, amorphous glass is not amenable to high temperature leaching [56]. Instead, pyrometallurgical options may be more appropriate for the Zeehan slag, with Verscheure et al. [57] describing two fuming processes (utilising IsaMelt technology) for treatment of Zn-bearing wastes. Such fuming technologies are commercially operational (e.g., Port Pirie, Australia) where zinc oxide is produced as the final product, and could be an option for this site to extract maximum value from these fine-grained, heterogeneous slags.

5.2.2. Biological Extraction

Whilst chemical leaching is a more conventional and time efficient process compared to bioleaching, silica gels can form, impacting leachate viscosity, as is the case when there is an abundance of silicate phases [58]. Removal of silica from the leachate is a technical challenge, though methodologies have been developed to overcome this, but ultimately they introduce additional steps in the process. Alternatively, an acid generating process involving bioleaching, which uses microorganisms to transform the solid compounds into soluble elements for recovery, could be used [59,60]. Potysz [58] recently undertook a review on the applications of bioleaching for metal recovery from slag. They summarised several case studies where experimental work was done on Pb–Zn slags from China, which were bioleached using *Bacillus*, *Sporosarcina* and *Pseudomonas*, with between 80% and 97% Zn extracted in 6 days. Bioleaching efficiency is increased if mixed cultures are used, as demonstrated by Kaksonen [61], who used *Acidithiobacillus ferrooxidans*, *Acidithiobacillus thiooxidans*, *Acidithiobacillus caldus*, *Leptospirillum ferrooxidans* and *Sulfobacillus thermotolerans* and later *Acidithiobacillus ferrivorans*, *Alicyclobacillus cycloheptanicus*, *Alicyclobacillus tolerans* and *Alicyclobacillus herbarium* [62] to bioleach Cu from slag collected at the Boliden Harjavalta Cu smelter. Potysz [58] proposed several generic bioleaching flowsheets for slag processing, and, based on their initial calculations, bioleaching was reported to be approximately three times more expensive than abiotic processing. However, Potysz [58] argued that the advantage of adopting a biotic approach is that it is a low-carbon technology with a cleaner final residue. In the case of Zeehan, bioleaching test work could be undertaken to determine

the optimum operating parameters (i.e., bacterial consortium to use, pH, nutrient content, pulp density, temperature) to enhance Zn recovery. Consideration too for the management of As in the waste residue should also be a priority, as it dominantly resides in Sulfide B (37%) and Glass A (34%).

5.2.3. Site Remediation

Regardless of the manner in which the Zeehan slags are processed, ultimately, the eventual remediation of the site must be a priority of any future work at this site, with a focus on remediating the contaminated topsoil (upon which the slag was dumped). When comparing the measured Zn in slag (average 111,000 mg/kg and 150,000 mg/kg for the North and South piles, respectively) against health-based investigation levels (HILs; NEPC, 2013 [63]), Zn values are 30,000 mg/kg (or 3 wt. %) if the final land use is a public open space (i.e., recreational use), and 400,000 mg/kg (or 40 wt. %) if for industrial use. Based on these values, if the final post-rehabilitation use for Zeehan is recreational, then adjacent soils are likely to be impacted, with adverse biological effects likely (e.g., death of vegetation, decreases in natural bacterial species and biomass, and health issues in humans [64]). Lead (average 20,000 mg/kg and 15,000 mg/kg for the North and South piles, respectively) is also elevated with respect to recreation and industrial HILs (600 mg/kg and 1500 mg/kg respectively). Arsenic (average 416 mg/kg and 384 mg/kg for the North and South piles respectively) only exceeds the recreational HIL value (300 mg/kg), and Cu (average 2000 mg/kg for both the North and South piles) does not exceed either HIL value (recreational: 17,000 mg/kg and industrial: 240,000 mg/kg). To treat the underlying soil, several options could be considered, including mineral addition (e.g., apatite for Pb and As removal [64,65]), biotic removal [59]; application of ferrihydrite to reduce Pb uptake in vegetation [64,66], and removal of contaminated topsoil or the emplacement of an engineered cover. Additionally, mapping of subsurface contamination (i.e., infiltration into the underlying Gordon Limestone) should form part of future work at the site. However, as with other historical mine waste sites in Tasmania (e.g., Savage River mine, Mt. Lyell mine) future efforts will require committed collaboration between the Tasmanian State Government and the current mining leaseholders to define the scope of rehabilitation works.

6. Conclusions

Metal liberation and sulfide oxidation from mine wastes can lead to the production and dispersal of AMD, its impacts and other metal transport mechanisms (e.g., dust dispersal) presenting significant management challenges at abandoned or historic mine and mineral processing sites. With many billions of tonnes of slag wastes present globally, understanding the properties of these materials is critical. Using the example of the Zeehan smelter site, this study has demonstrated that by adopting a geometallurgical approach to characterization (involving the integration of mineralogical and chemical datasets), potential rehabilitation options may be more readily defined. This site formerly processed ore from multiple metallurgical feed sources, with heterogeneous mineralogy and textures observed in these materials at both a macro- and micro-scale. The aim of this study was primarily to determine if slag reprocessing may be an option by examining element deportment within the different mineral phases present in this metallurgical waste.

The slag dumps at Zeehan (North and South piles), containing 46,900 t of material, have been surficially weathering since 1896, and are composed of air cooled slag with a diversity of texture influenced by the climatic regime experienced in Western Tasmania (i.e., heavy rainfall experienced from May to October). The North and South piles have a bulk Zn content of 11% and 15%, respectively. Mineralogically, the analysed samples are diverse, but contain phases resembling olivines, pyroxenes, glass, oxides and sulfides (e.g., fayalite–tephroite, kirschsteinite, franklinite, litharge, sphalerite and galena). The bulk mineralogy of the slag is comparable to other non-ferrous Pb–Zn slags from blast furnace operations during the 19th and 20th centuries. Zn in this material is partitioned into mineral phases resembling sulfides, silicates, oxides and glass, with Zeehan slag demonstrating similar properties to the the Hegeler Zn slag, Illinois, USA [33]. The high proportion of Zn partitioned into

sulfides (26%) has the potential to contribute to ground and surface water contamination, as sulfides are more reactive in nature than silicates and oxides [33], with observations of ephemeral goslarite ($ZnSO_4 \cdot 7H_2O$) at the surface of these piles, causing seasonally high loads of Zn to enter Austral Creek. Further, geo-environmental testing indicated that the Zeehan slag is potentially acid forming, with maximum potential acidity values ranging from 76.5 to 147 kg H_2SO_4/t, with weakly-acidic to circum-neutral paste pH values (pH 5 to 7). Other geo-environmental observations made at this site [23] confirm the potentially environmentally damaging nature of these materials. This study shows that because high concentrations of refractory Zn deport to several phases, a multi-staged recovery process using an integrated (bio)hydrometallurgical or pyrometallurgical approach to target the glass, sulfides, silicates and oxides should be designed to optimize results at Zeehan. Additional consideration to also recovering Ag, Pb and Cu should be given, as well as cost effectively managing Fe and As. The economics of reprocessing are currently being examined. The biggest challenge facing any further reprocessing plan is likely to be societal, as the site is regarded as a mining heritage site of interest with a contaminant footprint. Thus, further ground works at the former smelter site need to be undertaken with ongoing State Government and community consultation.

Supplementary Materials: The following are available online at http://www.mdpi.com/2075-163X/9/7/415/s1, Figure S1: Climate data for Zeehan, Figure S2: Example LA-ICP-MS spectrum for a silicate phase showing iron and zinc as homogenous elements; Table S1: Chemical data for the slag materials collected at the North and South piles, Zeehan, Table S2: Leachate chemistry of Zeehan slag; Table S3: Element concentrations measured by LA-ICPMS (values given in mg/kg) in slag mineral-like phases.

Author Contributions: Conceptualization, A.P.-F.; Methodology, S.G.; Software, S.G. and P.O.; Formal analysis, S.G and A.P.-F. and P.O.; Investigation, S.G.; Resources, A.P.-F.; Data curation, S.G.; Writing—original draft preparation, A.P.-F..; Writing—review and editing, A.P.-F. and N.F.; Supervision, A.P.-F. and P.O. and N.F.; Project administration, A.P.-F.; Funding acquisition, A.P.-F. and S.G.

Funding: This research was funded by Australian Research Council's Industrial Research Hub for Transforming the Mining Value Chain (project number IH130200004). Additional funding was provided to S.G from Mineral Resources Tasmania, AusIMM, Geological Society of Australia and MMG Limited.

Acknowledgments: Acknowledgments go to Helen Scott at the ARC TMVC Hub members for project administration, Sandrin Feig (CSL) for SEM assistance, Ashley Townsend (CSL) for ICP-MS analysis and Laura Jackson (RGS) for geochemical laboratory assistance. We also thank Kim Denwar (MMG Limited), Andrew McNeil (MRT) and Karin Orth (GSA-Tas secretary) for organising analyses and providing extra funds. A special thanks goes to Josh Denholm (UTAS) for field assistance during the sampling campaign. We thank the two anonymous reviewers for their extremely helpful review comments; these were most insightful and constructive.

Conflicts of Interest: The authors declare no conflict of interest.

References

1. Velenturf, A.P.M.; Jopson, J.S. Making the business case for resource recovery. *Sci. Total Environ.* **2019**, *648*, 1031–1041. [CrossRef] [PubMed]
2. Bleicher, A.; David, M.; Rutjes, H. When environmental legacy becomes a resource: On the making of secondary resources. *Geoforum* **2019**, *101*, 18–27. [CrossRef]
3. Afum, B.D.; Caverson, D.; Ben-Awuah, E. A conceptual framework for characterizing mineralized waste rocks as future resource. *Int. J. Min. Sci. Technol.* **2019**, *29*, 429–435. [CrossRef]
4. Young, J.E. *Mining the Earth*; WorldWatch: Washington, DC, USA, 1992.
5. Jenkins, H.; Yakovleva, N. Corporate social responsibility in the mining industry: Exploring trends in social and environmental disclosure. *J. Clean. Prod.* **2006**, *14*, 271–284. [CrossRef]
6. Parbhakar-Fox, A.K.; Edraki, M.; Hardie, K.; Kadletz, O.; Hall, T. Identification of acid rock drainage sources through mesotextural classification at abandoned mines of Croydon, Australia: Implications for the rehabilitation of waste rock repositories. *J. Geochem. Explor.* **2014**, *137*, 11–28. [CrossRef]
7. Griggs, D.; Stafford-Smith, M.; Gaffney, O.; Rockström, J.; Öhman, M.C.; Shyamsundar, P.; Steffen, W.; Glaser, G.; Kanie, N.; Noble, I. Policy: Sustainable development goals for people and planet. *Nature* **2013**, *495*, 305–307. [CrossRef] [PubMed]
8. Piatak, N.M.; Parsons, M.B.; Seal, R.R., II. Characteristics and environmental aspects of slag: A review. *Appl. Geochem.* **2015**, *57*, 236–266. [CrossRef]

9. Lottermoser, B.G. Evaporative mineral precipitates from a historical smelting slag dump, Rio Tinto, Spain. *Neues Jahrbuch für Mineralogie-Abhandlungen* **2005**, *181*, 183–190. [CrossRef]
10. Piatak, N.M. Environmental characteristics and utilization potential of metallurgical slag. In *Environmental Geochemistry*, 2nd ed.; Elsevier: Amsterdam, The Netherlands, 2018; pp. 487–519.
11. Csavina, J.; Field, J.; Taylor, M.P.; Gao, S.; Landázuri, A.; Betterton, E.A.; Sáez, A.E. A review on the importance of metals and metalloids in atmospheric dust and aerosol from mining operations. *Sci. Total Environ.* **2012**, *433*, 58–73. [CrossRef]
12. Pugin, K.G.; Vaysman, Y.I. Methodological approaches to development of ecologically safe usage technologies of ferrous industry solid waste resource potential. *World Appl. Sci. J.* **2013**, *22*, 28–33. [CrossRef]
13. Available online: http://www.euroslag.com (accessed on 11 April 2019).
14. Australasian Slag Association. Available online: http://www.asa-inc.org.au (accessed on 1 April 2019).
15. Roberts, G. *Metal Mining in Tasmania, 1804 to 1914: How Government Helped Shape the Mining Industry*; Bookprint Pty. Limited: Launceston, Australia; Fullers Bookshop: Launceston, Australia, 2007.
16. Williams, K.; Both, R. *Geological Survey Record No. 11 Mineralogy of the Mines and Prospects of the Zeehan Field*; Mineral Resources Tasmania; Government Printer: Hobart, Tasmania, 1971.
17. Solomon, M. An introduction to the geology and metallic ore deposits of Tasmania. *Econ. Geol.* **1981**, *76*, 194–208. [CrossRef]
18. Seymour, D.B.; Green, G.R.; Calver, C.R. *The Geology and Mineral Deposits of Tasmania: A Summary*; Mineral Resources Tasmania: Rosny Park, Australia, 2006.
19. Fox, N.; Parbhakar-Fox, A.; Lottermoser, B. Prediction of Metal Mobility from Sulfidic Waste Rocks Using Micro-Analytical Tools, Spray, Tasmania. In *Environmental Indicators in Metal Mining*; Springer: Cham, Switzerland, 2017; pp. 263–277.
20. Bacon, C.A. A Tasmanian mining history timeline. In *Tasmanian Geological Survey Record 2013/10*; Mineral Resources Tasmania: Sydney, Australia, 2013.
21. Blissett, A.H. *Geological Survey Explanatory Report: One Mile Geological Map Series, K'55-5-50, Zeehan*; Tasmania Department of Mines: Hobart, Australia, 1962.
22. Brown, A.; Findlay, R.; Goscombe, B.; McClenaghan, M.; Seymore, D. *Geological Atlas 1: 50 000 Series. Sheet 50 (7914S), Zeehan*; Mineral Resources Tasmania: Sydney, Australia, 2004.
23. Taylor, K. *Acid Drainage Abatement from an Abandoned Smelter Site, Zeehan*; University of Tasmania: Hobart, Australia, 1998.
24. Dold, B. Speciation of the most soluble phases in a sequential extraction procedure adapted for geochemical studies of copper sulfide mine waste. *J. Geochem. Explor.* **2003**, *80*, 55–68. [CrossRef]
25. Noble, T.L.; Lottermoser, B.G.; Parbhakar-Fox, A. Evaluation of pH testing methods for sulfidic mine waste. *Mine Water Environ.* **2015**, *35*, 318–331. [CrossRef]
26. Smart, R.; Skinner, W.; Levay, G.; Gerson, A.; Thomas, J.; Sobieraj, H.; Schumann, R.; Weisener, C.; Weber, P.; Miller, S. *ARD Test Handbook: Project P387, A Prediction and Kinetic Control of Acid Mine Drainage*; Ian Wark Research Institute: Melbourne, Australia, 2002.
27. Parbhakar-Fox, A.; Lottermoser, B. *Predictive Environmental Indicators in Mining: Review of the Literature and Current Best Practices*; CRC ORE Technical Report 2; CRC for Optimising Resource Extraction: Brisbane, Australia, 2011.
28. Parbhakar-Fox, A.; Fox, N.; Ferguson, T.; Hill, R.; Maynard, B. Dissection of the NAG pH test: Tracking efficacy through examining reaction products. In Proceedings of the 11th International Conference on Acid Rock Drainage 2018, Pretoria, South Africa, 10–14 September 2018; pp. 949–955.
29. Norris, A.; Danyushevsky, L. *Towards Estimating the Complete Uncertainty Budget of Quantified Results Measured by LA-ICPMS*; Goldschmidt: Boston, MA, USA, 2018.
30. Schindler, M. A mineralogical and geochemical study of slag from the historical O'Donnell Roast Yards, Sudbury, Ontario, Canada. *Can. Miner.* **2014**, *52*, 433–452. [CrossRef]
31. Ettler, V.; Legendre, O.; Bodénan, F.; Touray, J.C. Primary phases and natural weathering of old lead–zinc pyrometallurgical slag from Příbram, Czech Republic. *Can. Miner.* **2001**, *39*, 873–888. [CrossRef]
32. Bell, R.C.; Turner, G.H.; Peters, E. Fuming of zinc from lead blast slag furnace. *JOM* **1955**, *7*, 472–477. [CrossRef]
33. Piatak, N.M.; Seal, R.R., II. Mineralogy and the release of trace elements from slag from the Hegeler Zinc smelter, Illinois (USA). *Appl. Geochem.* **2010**, *25*, 302–320. [CrossRef]

34. Puziewicz, J.; Zainoun, K.; Bril, H. Primary phases in pyrometallurgical slags from a zinc-smelting waste dump, S'wietochłowice, Upper Silesia, Poland. *Can. Miner.* **2007**, *45*, 1189–1200. [CrossRef]
35. Tyszka, R.; Kierczak, J.; Pietranik, A.; Ettler, V.; Mihaljevič, M. Extensive weathering of zinc smelting slag in a heap in Upper Silesia (Poland): Potential environmental risks posed by mechanical disturbance of slag deposits. *Appl. Geochem.* **2014**, *40*, 70–81. [CrossRef]
36. Weber, P.; Hughes, J.B.; Conner, L.B.; Lindsay, P.; Smart, R.S.C. *Short Term Acid Drainage Characteristics Determined by Paste pH and Kinetic NAG Testing: Cypress Prospect*; American Society of Mining and Reclamation (ASMR): St. Louis, MO, USA, 2006.
37. Lahiri, P.; Sengupta, S.K. Spinel ferrites as catalysts: A study on catalytic effect of co-precipitated ferrites on hydrogen peroxide decomposition. *Can. J. Chem.* **1991**, *69*, 33–36. [CrossRef]
38. Seal, R.; Foley, N.K.; Wanty, R.B. Introduction to geoenvironmental models of mineral deposits U.S. Geological Survey Open-File Report 02-195; Chapter A; pp. 1–7. Available online: https://pubs.usgs.gov/of/2002/of02-195/OF-02-195-508-V5.pdf (accessed on 5 July 2019).
39. Australia and New Zealand Guidelines for Fresh and Marine Water Quality. 2000. Available online: https://www.waterquality.gov.au/sites/default/files/documents/anzecc-armcanz-2000-guidelines-vol1.pdf (accessed on 15 June 2019).
40. Ficklin, W.H.; Plumlee, G.S.; Smith, K.S.; McHugh, J.B. Geochemical classification of mine drainages and natural drainages in mineralised areas. In Proceedings of the 7th International Water-Rock Interaction Conference, Park City, UT, USA, 13–18 July 1992.
41. Gbor, P.K.; Mokri, V.; Jia, C.Q. Characterization of smelter slags. *J. Environ. Sci. Health A* **2000**, *35*, 147–167. [CrossRef]
42. Ettler, V.; Červinka, R.; Johan, Z. Mineralogy of medieval slags from lead and silver smelting (Bohutín, Příbram district, Czech Republic): Towards estimation of historical smelting conditions. *Archaeometry* **2009**, *51*, 987–1007. [CrossRef]
43. Piatak, N.M.; Seal, R.R., II. Mineralogy and environmental geochemistry of historical iron slag, Hopewell Furnace, national historic site, Pennsylvania, USA. *Appl. Geochem.* **2012**, *27*, 623–643. [CrossRef]
44. Shannon, R.D.; Prewitt, C.T. Revised values of effective ionic radii. *Acta Crystallogr. B* **1970**, *26*, 1046–1048. [CrossRef]
45. Ettler, V.; Johan, Z.; Touray, J.C.; Jelínek, E. Zinc partitioning between glass and silicate phases in historical and modern lead–zinc metallurgical slags from the Příbram district, Czech Republic. *C. R. Acad. Sci.* **2000**, *331*, 245–250. [CrossRef]
46. Lockington, J.A.; Cook, N.J.; Ciobanu, C.L. Trace and minor elements in sphalerite from metamorphosed sulfide deposits. *Miner. Petrol.* **2014**, *108*, 873–890. [CrossRef]
47. Tyszka, R.; Pietranik, A.; Kierczak, J.; Zieliński, G.; Darling, J. Cadmium distribution in Pb-Zn slags from Upper Silesia, Poland: Implications for cadmium mobility from slag phases to the environment. *J. Geochem. Explor.* **2018**, *186*, 215–224. [CrossRef]
48. Jambor, J.L. Mine-waste mineralogy and mineralogical perspectives of acid–base accounting. In *Environmental Aspects of Mine Wastes*; Jambor, J.L., Blowes, D.W., Ritchie, A.I.M., Eds.; Mineralogical Association of Canada: Nepean, ON, Canada, 2003.
49. Parsons, M.B.; Bird, D.K.; Einaudi, M.T.; Alpers, C.N. Geochemical and mineralogical controls on trace element release from the Penn Mine base-metal slag dump, California. *Appl. Geochem.* **2001**, *16*, 1567–1593. [CrossRef]
50. Piatak, N.M.; Seal, R.K.; Hammarstrom, J.M. Mineralogical and geochemical controls on the release of trace elements from slag produced by base-and precious-metal smelting at abandoned mine sites. *Appl. Geochem.* **2004**, *19*, 1039–1064. [CrossRef]
51. Pan, J.; Plant, J.A.; Voulvoulis, N.; Oates, C.J.; Ihlenfeld, C. Cadmium levels in Europe: Implications for human health. *Environ. Geochem. Health* **2010**, *32*, 1–12. [CrossRef]
52. Cundy, A.B.; Bardos, R.P.; Church, A.; Puschenreiter, M.; Friesl-Hanl, W.; Müller, I.; Neu, S.; Mench, M.; Witters, N.; Vangronsveld, J. Developing principles of sustainability and stakeholder engagement for "gentle" remediation approaches: The European context. *J. Environ. Econ. Manag.* **2013**, *129*, 283–291. [CrossRef] [PubMed]

53. Schneider, L.; Mariani, M.; Saunders, K.M.; Maher, W.A.; Harrison, J.J.; Fletcher, M.S.; Zawadzki, A.; Heijnis, H.; Haberle, S.G. How significant is atmospheric metal contamination from mining activity adjacent to the Tasmanian Wilderness World Heritage Area? A spatial analysis of metal concentrations using air trajectories models. *Sci. Total Environ.* **2019**, *656*, 250–260. [CrossRef] [PubMed]
54. Kurama, H.; Goektepe, F. Recovery of zinc from waste material using hydro metallurgical processes. *Environ. Prog.* **2003**, *22*, 161–166. [CrossRef]
55. Ma, A.; Zheng, X.; Li, S.; Wang, Y.; Zhu, S. Zinc recovery from metallurgical slag and dust by coordination leaching in NH_3–CH_3COONH_4–H_2O system. *R. Soc. Open Sci.* **2018**, *5*, 180660. [CrossRef] [PubMed]
56. Perederiy, I.; Papangelakis, V.G. Why amorphous FeO-SiO_2 slags do not acid leach at high temperatures. *J. Hazard. Mater.* **2017**, *321*, 737–744. [CrossRef] [PubMed]
57. Verscheure, K.; Camp, M.V.; Blanpain, B.; Wollants, P.; Hayes, P.C.; Jak, E. Investigation of zinc fuming processes for the treatment of zinc-containing residues. In Proceedings of the International Symposium on Sustainable Developments in Metals Processing, Melbourne, Australia, 3–6 July 2005.
58. Potysz, A.; Hullebusch, E.D.; Kierczak, J. Perspectives regarding the use of metallurgical slags as secondary metal resources—A review of bioleaching approaches. *J. Environ. Manag.* **2018**, *219*, 138–152. [CrossRef] [PubMed]
59. Cheng, Y.; Guo, Z.; Liu, X.; Yin, H.; Qiu, G.; Pan, F.; Liu, H. The bioleaching feasibility for Pb/Zn smelting slag and community characteristics of indigenous moderate-thermophilic bacteria. *Bioresour. Technol.* **2009**, *100*, 2737–2740. [CrossRef] [PubMed]
60. Guo, Z.; Zhang, L.; Cheng, Y.; Pan, F.; Jiang, K. Effects of pH, pulp density and particle size on solubilization of metals from a Pb/Zn smelting slag using indigenous moderate thermophilic bacteria. *Hydrometallurgy* **2010**, *104*, 25–31. [CrossRef]
61. Kaksonen, A.H.; Lavonen, L.; Kuusenaho, M.; Kolli, A.; Närhi, H.; Vestola, E.; Puhakka, J.A.; Tuovinen, O.H. Bioleaching and recovery of metals from final slag waste of the copper smelting industry. *Min. Eng.* **2011**, *24*, 1113–1121. [CrossRef]
62. Kaksonen, A.H.; Sarkijarvi, S.; Puhakka, J.A.; Peuraniemi, E.; Junnikkala, S.; Tuovinen, O.H. Chemical and bacterial leaching of metals from a smelter slag in acid solutions. *Hydrometallurgy* **2016**, *159*, 46–53. [CrossRef]
63. National Environment Protection (Assessment of Site Contamination) Guidelines on Investigation for Soil and Groundwater. 2011. Available online: http://www.nepc.gov.au/system/files/resources/93ae0e77-e697-e494-656f-afaaf9fb4277/files/schedule-b1-guideline-investigation-levels-soil-and-groundwater-sep10.pdf (accessed on 12 June 2019).
64. Chen, X.; Wright, J.V.; Conca, J.L.; Peurrung, L.M. Evaluation of heavy metal remediation using mineral apatite. *Water Air Soil Pollut.* **1997**, *8*, 57–78. [CrossRef]
65. Ma, Q.Y.; Traina, S.J.; Logan, T.J.; Ryan, J.A. In situ lead immobilization by apatite. *Environ. Sci. Technol.* **1993**, *27*, 1803–1810. [CrossRef]
66. Friesl, W.; Friedl, J.; Platzer, K.; Horak, O.; Gerzabek, M.H. Remediation of contaminated agricultural soils near a former Pb/Zn smelter in Austria: Batch, pot and field experiments. *Environ. Pollut.* **2006**, *144*, 40–50. [CrossRef] [PubMed]